Three-dimensional semi-idealized model for estuarine turbidity maxima in tidally dominated estuaries

Kumar, Mohit; Schuttelaars, Henk M.; Roos, Pieter C.

DOI
10.1016/j.ocemod.2017.03.005

Publication date
2017

Document Version
Final published version

Published in
Ocean Modelling

Ocean Modelling 113 (2017) 1–21

Contents lists available at ScienceDirect

Ocean Modelling

journal homepage: www.elsevier.com/locate/ocemod

Virtual Special Issue
Coastal ocean modelling

Three-dimensional semi-idealized model for estuarine turbidity maxima in tidally dominated estuaries

Mohit Kumar[a,*], Henk M. Schuttelaars[a], Pieter C. Roos[b]

[a] Delft Institute of Applied Mathematics, Delft University of Technology, The Netherlands
[b] Department of Water Engineering and Management, University of Twente, The Netherlands

ARTICLE INFO

Article history:
Received 12 June 2016
Revised 16 February 2017
Accepted 5 March 2017
Available online 6 March 2017

Keywords:
Idealized model
Morphodynamic equilibrium
Estuarine turbidity maxima
Ems estuary

ABSTRACT

We develop a three-dimensional idealized model that is specifically aimed at gaining insight in the physical mechanisms resulting in the formation of estuarine turbidity maxima in tidally dominated estuaries. First, the three-dimensional equations for water motion and suspended sediment concentration together with the so-called morphodynamic equilibrium condition, are scaled. Next, surface elevation, velocity and sediment concentration are expanded in a small parameter $\epsilon = \bar{A}_{M_2}/H$, where $\bar{A}_{M_2}$ is the mean amplitude of the M_2 tide and H is the mean water depth at the seaward side. This results in a system of equations at each order in this small parameter. This ordering allows solving for the vertical structure of the velocity and suspended sediment concentration, independently of the horizontal dimension. After obtaining these vertical structures, the horizontal dependencies of the physical variables follow from solving a two-dimensional elliptic partial differential equation for the surface elevation. The availability of fine sediments in the estuary follows from a two-dimensional elliptic partial differential equation which results from requiring the system to be in morphodynamic equilibrium, and prescribing the total amount of easily erodible sediments available in the estuary. These elliptic equations for the surface elevation and sediment availability are solved numerically using the finite element method with cubic polynomials as basis functions. As a first application, the model is applied to the Ems estuary using a simplified geometry and bathymetric profiles characteristic for the years 1980 and 2005. The availability of fine sediments and location of maximum concentration are investigated for different lateral depth profiles. In the first experiment, a uniform lateral depth is considered. In this case, both the sediment availability and suspended sediment concentration are, as expected, uniform in the lateral direction. In 1980, the sediment is mainly trapped near the entrance, while in 2005, the sediment is mostly trapped in the freshwater zone. In the next experiment, the lateral bathymetry is varied parabolically while keeping the mean depth unchanged. In this case, the fine sediment is mainly found at the shallow sides, but the maximum sediment concentration is found in the deeper channel where the bed shear stress is much larger than on the shoals. As a final experiment, a more realistic (but smoothed) geometry and bathymetry for the Ems estuary are considered, showing the possibilities of applying the newly developed model to complex geometries and bathymetries.

1. Introduction

In most estuaries, regions are observed with elevated suspended sediment concentration compared with the adjacent landward and seaward regions. These regions are called *estuarine turbidity maxima* (ETM). A good understanding of the ETM dynamics is important for many reasons (for a detailed discussion, see Jay et al., 2015). First, the presence of an ETM can have a strong influence on the ecological functioning of an estuary, as it can result in limited light conditions or anoxia (Talke et al., 2009b). Furthermore, at the location of the ETM, there is often a considerable deposition of fine sediments, which results in enhanced dredging

* Corresponding author.
E-mail addresses: m.kumar@tudelft.nl (M. Kumar), h.m.schutteraars@tudelft.nl (H.M. Schuttelaars), p.c.roos@utwente.nl (P.C. Roos).

http://dx.doi.org/10.1016/j.ocemod.2017.03.005
1463-5003/

efforts to keep the estuary accessible and the navigation lanes at their regular depths. Finally, ETM dynamics is shown to be sensitive to changes in bathymetry, geometry and external forcing conditions (de Jonge et al., 2014), which (if not well understood) can result in a deterioration of the system as a whole.

To better understand and assess the effects of natural or anthropogenic changes on ETM dynamics, different types of models are being applied (Murray, 2003). For example, state-of-the-art three dimensional process-based models are applied to simulate ETM dynamics (Weilbeer, 2008; van Maren et al., 2015) and changes in ETM dynamics due to human interventions. However, these models are computationally expensive and the mechanisms resulting in the observed dynamics are difficult to analyse (Schuttelaars et al., 2013).

Alternatively, process-based idealized models are specifically designed to and aimed towards studying the mechanisms resulting in the formation of ETMs and assessing their sensitivity to parameters. Since these models focus on a specific phenomenon, some processes are not or only parametrically taken into account. Furthermore, geometry and bathymetry are often simplified. Huijts et al. (2006) used an idealized modelling approach to study the trapping of fine sediments in the lateral direction. Talke et al. (2009a) and Chernetsky et al. (2010) focused on the sediment transport in the longitudinal direction, using a width-averaged model. However, Geyer et al. (1998) and Kim and Voulgaris (2008) pointed out that the lateral water motion and suspended sediment dynamics affect the processes in the longitudinal direction and vice-versa. Therefore, to understand the ETM dynamics and the underlying dominant trapping mechanisms (see for example Jay et al., 2015 for an overview of possible mechanisms), it is necessary to study both the lateral and longitudinal processes simultaneously. Clearly, this requires a three-dimensional modelling approach.

For the water motion, three-dimensional idealized models have been developed and analysed in detail (Winant, 2007; 2008; Ensing et al., 2015; Kumar et al., 2016), but for the sediment transport and trapping of fine sediments, three-dimensional idealized models are still missing. Therefore, the aim of this paper is to develop a three-dimensional idealized model for water motion and sediment dynamics in an estuary of arbitrary shape and bathymetry, including the Coriolis effect. This allows for a systematic study of the sediment trapping mechanisms in a tidally-dominated estuaries. The physical parameters are allowed to vary in the horizontal plane. The three-dimensional model is solved using an asymptotic expansion technique. This results in analytic solutions of the vertical profiles of the velocity and suspended sediment concentration. These solutions still depend on the (gradients of the) surface elevation. The surface elevation itself follows from a two-dimensional elliptic partial differential equation which is solved numerically using the finite element method. The condition of morphodynamic equilibrium is prescribed to govern the availability of fine sediments in the estuary.

As a first example, the new model is applied to the Ems estuary using simplified geometric and bathymetric profiles characteristic for 1980 and 2005. The location of maximum trapping of sediments for both years is investigated. The influence of lateral bathymetry is investigated by first keeping the depth in the lateral direction uniform. Next, the lateral bathymetric profile is varied parabolically while keeping the width-averaged depth unchanged. The results are qualitatively compared with observations and the influence of lateral depth variations is discussed. As a final example, we use the (smoothed) observed bathymetry and geometry of the Ems in 2005 to obtain the trapping location of the fine sediments.

The structure of the paper is as follows. The philosophy of idealized modelling and step by step overview of model development are presented in Section 2. The model equations of water motion and suspended sediment concentration and the condition of morphodynamic equilibrium are presented in Section 3. This section also presents the scaling and perturbation analyses which results in a system of equations at each order for the water motion and the suspended sediment concentration. The leading-order system for the water motion is solved in Section 4, the first-order system in Section 5. Similarly, the leading-order and first-order systems for suspended sediment concentrations are solved in Sections 6 and 7, respectively. The equation for sediment availability governing the distribution of fine sediments in the estuary is solved in Section 8. Section 9 gives a short description of the numerical solution procedure for the two-dimensional elliptic partial differential equations obtained for both the surface elevation and sediment availability with a special discussion on the accuracy of the resulting solutions. Next, this model is applied to the Ems estuary in Section 10. Finally, conclusions are presented in section 11.

2. Idealized model - model philosophy

The main research question will be answered by developing a so-called *idealized, process-based model*. Idealized models focus on specific phenomena (here ETM formation), neglecting or simplifying processes that are not essential for the phenomenon under study. In this paper, we focus on developing such a model for a tidally dominated, well-mixed estuary. It is assumed that the suspended sediment concentrations do not influence the water motion significantly, and that the water motion is mainly driven by a prescribed M_2 tide at the seaward side.

In constructing this idealized model, ten steps can be identified. These steps are visualized in Fig. 1; the precise sections where the individual steps are discussed in detail, are indicated in this figure as well. Below, the main steps are summarized:

1. Derive the model equations, and define the geometry and bathymetry of interest.
2. Make the physical variables (such as surface elevation, water depth, etc.) dimensionless by introducing typical scales; subsequently use this to make the governing equations dimensionless. Since all dimensionless physical variables are order one, the relative importance of each term in any of the equations is measured by the magnitude of the dimensionless number, multiplying the dimensionless group of physical variables. These magnitudes can be calculated explicitly after choosing scales that are representative for the estuary/class of estuaries under consideration.
3. Verify that one of the dimensionless numbers is the ratio of the M_2 surface elevation averaged over the entrance (A_{M_2}) and the mean water depth H at the seaward boundary. This ratio, denoted by ϵ, is much smaller than one. Next, all other dimensionless numbers are related to ϵ.
4. Expand the physical variables in the small parameter ϵ. These asymptotic expansions are introduced in the dimensionless equations, and terms of equal order in ϵ are collected. Since only terms of equal order in ϵ can balance, this results in a system of equations at each order in ϵ.
5. Construct the solutions for the leading-order water motion, i.e., at order ϵ^0. Since the leading-order water motion is only driven by the M_2 tidal signal at the seaward boundary, it only consists of an M_2 constituent.
6. Derive the first-order water motion using the leading-order water motion, i.e., ϵ^1. It is found that the temporal variations of the first order water motion consist of a residual and an M_4 contribution.
7. Calculate the leading-order concentration using the leading-order water motion. Concerning its temporal behaviour, a resid-

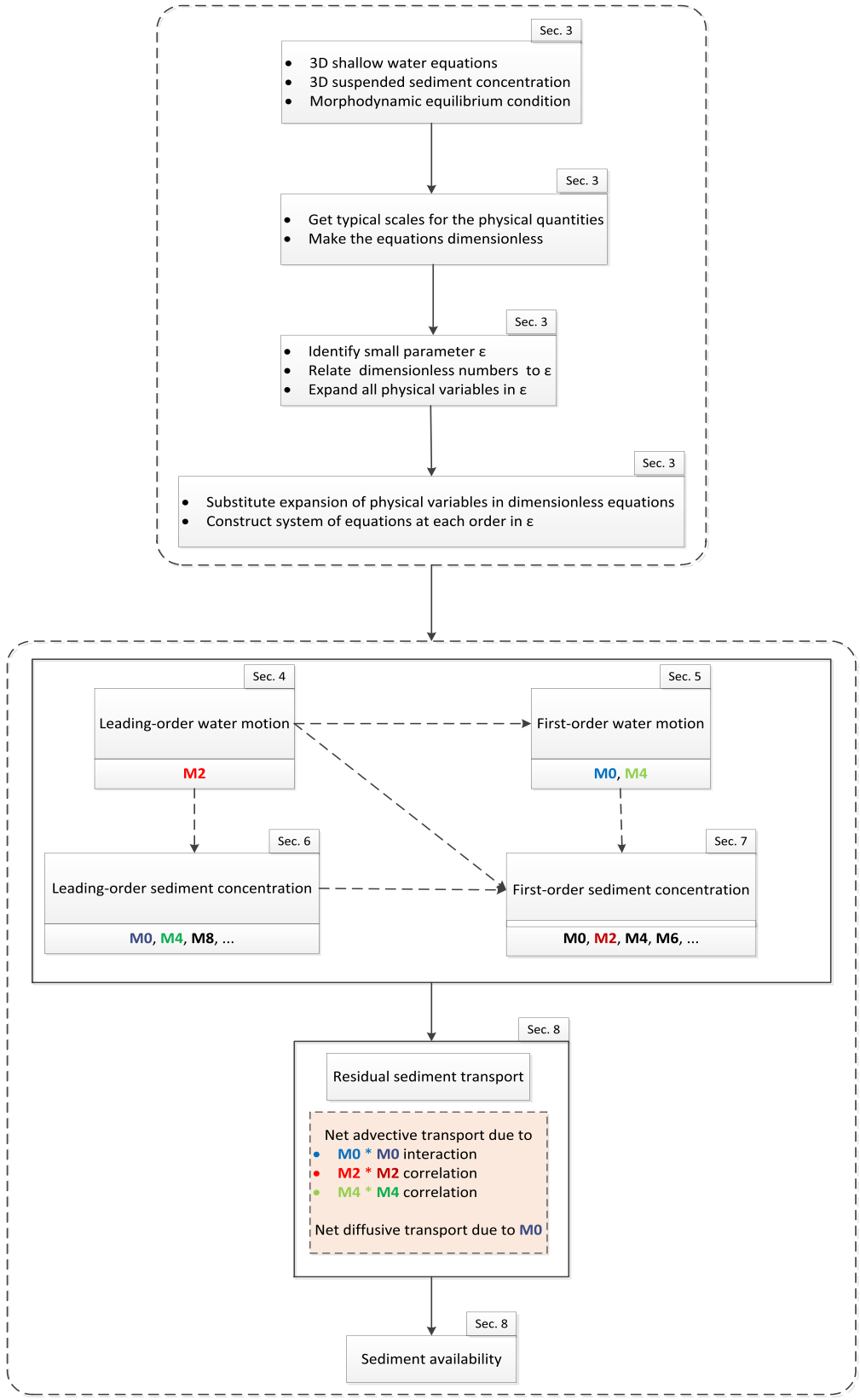

Fig. 1. Flow chart showing the steps involved in the development of the idealized model.

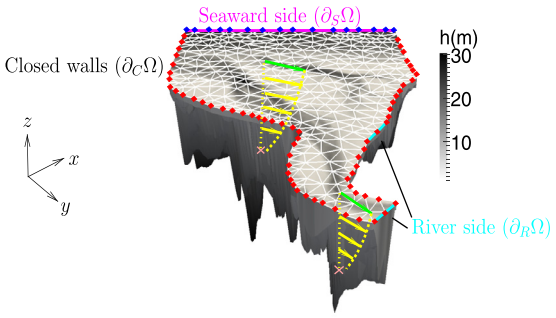

Fig. 2. Three-dimensional sketch of an estuary with arbitrary geometric and bathymetric profiles. The bathymetric profile is shown on a grayscale. The seaward side (denoted by $\partial_S\Omega$) is shown in magenta colour (——) and the river boundary (denoted by $\partial_R\Omega$) in cyan colour (——). The other boundaries (denoted by $\partial_C\Omega$) are assumed to be closed walls. The surface of the estuary is discretized using linear triangles in order to compute the surface elevation with the finite element method. The nodes on the seaward boundary (where elevation amplitude is prescribed) are indicated by blue diamonds (♦) and on rest of the boundaries (nodes where the surface elevation has to be computed) by red diamonds (♦). At each node in the triangulation of the surface, the vertical profile of the velocity field can be computed analytically using partial derivatives of the surface elevation as shown by yellow dashed lines (- - - - -). The velocity at the surface is depicted by green arrows (→) and, in the rest of the water column, by yellow arrows (→). This figure has been taken from Kumar et al. (2016). (For interpretation of the references to colour in this figure legend, the reader is referred to the web version of this article.)

ual contribution and contributions with multiples of the M_4 tidal frequency are obtained.

8. The first-order suspended sediment concentration is obtained using information of both the leading- and first-order velocity fields, and the leading-order concentration. The temporal variations of the first-order concentration consist of a residual contribution and contributions with multiples of the M_2 tidal frequency.
9. Calculate the leading-order, tidally averaged suspended sediment transport. It consists of three contributions:
   - advective transport due to correlations between the leading-order velocity and first-order concentration. Only the correlation between the leading-order velocity and the M_2 component of the first-order concentration results in a net transport.
   - advective transport due to correlations between the first-order velocity and leading-order concentration. Both the residual concentration, advected by the residual velocity, and the correlation between the first-order M_4 velocity and the M_4 component of the leading-order concentration result in a net transport.
   - diffusive transport due to spatial gradients in the residual concentration field.
10. Impose the condition of morphodynamic equilibrium to obtain the spatial distribution of easily erodible sediments.

In the following sections (see Fig. 1), these steps will be executed to develop a model for sediment trapping in a tidally-dominated estuary.

3. Model formulation

3.1. Model domain

An estuary of arbitrary shape (geometry) and depth profile (bathymetry) is considered (Fig. 2). A Cartesian coordinate system is used, with x, y denoting the horizontal coordinates, and z the vertical coordinate, pointing in the upward direction. Importantly, x or y need not represent the along-channel or cross-channel coordinate. The undisturbed water level is denoted by $z = 0$ and the surface elevation by $z = \eta(x, y, t)$, where t is time. The undisturbed bed level denoted by $z = -h(x, y)$, is assumed to be prescribed and independent of time on the time scale under consideration. Boundaries where the surface elevation is prescribed are called seaward boundaries (denoted by $\partial_S\Omega$), if river discharge is prescribed, they are called river boundaries (denoted by $\partial_R\Omega$). The closed boundaries are denoted by $\partial_C\Omega$.

3.2. Water motion

The water motion is governed by the three-dimensional shallow water equations, including the Coriolis effect. Conservation of mass and momentum (using the Boussinesq approximation and hydrostatic balance) is expressed as (Cushman-Roisin and Beckers, 2011; Vreugdenhil, 1994)

$$\frac{\partial u}{\partial x} + \frac{\partial v}{\partial y} + \frac{\partial w}{\partial z} = 0, \tag{1a}$$

$$\frac{\partial u}{\partial t} + u\frac{\partial u}{\partial x} + v\frac{\partial u}{\partial y} + w\frac{\partial u}{\partial z} - fv = -g\frac{\partial \eta}{\partial x} - \frac{g}{\rho_0}\int_z^\eta \frac{\partial \rho}{\partial x}\mathrm{d}z' + \frac{\partial}{\partial z}\left(A_v\frac{\partial u}{\partial z}\right), \tag{1b}$$

$$\frac{\partial v}{\partial t} + u\frac{\partial v}{\partial x} + v\frac{\partial v}{\partial y} + w\frac{\partial v}{\partial z} + fu = -g\frac{\partial \eta}{\partial y} - \frac{g}{\rho_0}\int_z^\eta \frac{\partial \rho}{\partial y}\mathrm{d}z' + \frac{\partial}{\partial z}\left(A_v\frac{\partial v}{\partial z}\right). \tag{1c}$$

The unknown variable $\boldsymbol{u} = (u, v, w)$ denotes the components of the velocity field in x, y and z directions, respectively. The mean density is denoted by ρ_0 and the dynamic density by $\rho(x, y)$ which is assumed to be a prescribed function of the horizontal coordinates x and y only, i.e., the estuary is assumed to be well-mixed. Furthermore, time variations in ρ are neglected. The vertical eddy viscosity coefficient is denoted by $A_v(x, y)$ and is assumed to be a prescribed function of x and y only, thus uniform in z and time-invariant. Note that horizontal viscous effects are neglected in Eq. (1), see Winant (2007) for a detailed discussion. The parameter f is the Coriolis parameter, given by $f = 2\tilde{\Omega}\sin\theta$, where $\tilde{\Omega} = 7.292 \times 10^{-5}$ rad s^{-1} is the angular frequency of the Earth's rotation, and θ the latitude which is assumed to be uniform over the domain (f-plane approximation).

To obtain a well-posed problem for the water motion, appropriate boundary conditions have to be prescribed. At the seaward boundary ($\partial_S\Omega$), the system is forced with a combination of a prescribed semi-diurnal lunar (M_2) tide and its first overtide (M_4),

$$\eta = A_{M_2}\cos(\omega t - \phi_{M_2}) + A_{M_4}(2\omega t - \phi_{M_4}), \quad \text{for all } (x, y) \text{ in } \partial_S\Omega, \tag{2a}$$

where $A_{M_2}(x, y)$ and $A_{M_4}(x, y)$ are the (possibly) spatially varying amplitudes of the surface elevation of the M_2 and M_4 tidal constituents at the seaward boundary. The phases of the M_2 and M_4 tides at the seaward side are denoted by $\phi_{M_2}(x, y)$ and $\phi_{M_4}(x, y)$, respectively. The M_2 tidal constituent is assumed to be the dominant one, i.e., $A_{M_4} < A_{M_2}$. The parameter $\omega = 2\pi/T$ denotes the angular frequency of the M_2 tide with period $T = 12.42$ h. At the river boundary ($\partial_R\Omega$), a time-independent river discharge Q (m^3 s^{-1}) is prescribed,

$$\int_{\partial_R\Omega}\left(\int_{-h}^{\eta}\boldsymbol{u}_h\cdot\hat{\mathbf{n}}\,\mathrm{d}z\right)\mathrm{d}s = -Q, \tag{2b}$$

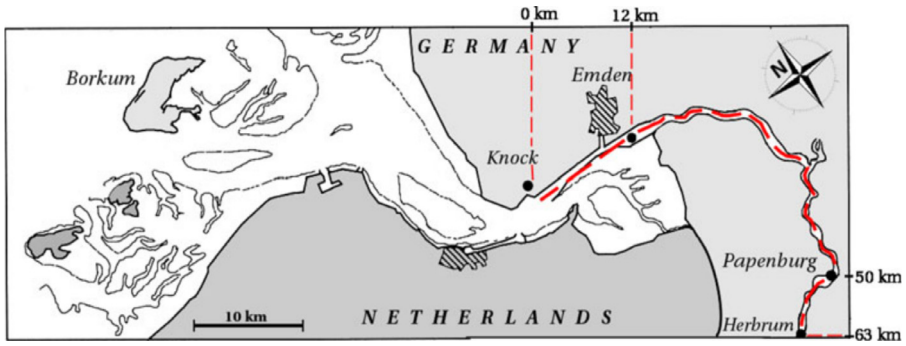

Fig. 3. The map of the Ems estuary (Chernetsky et al., 2010).

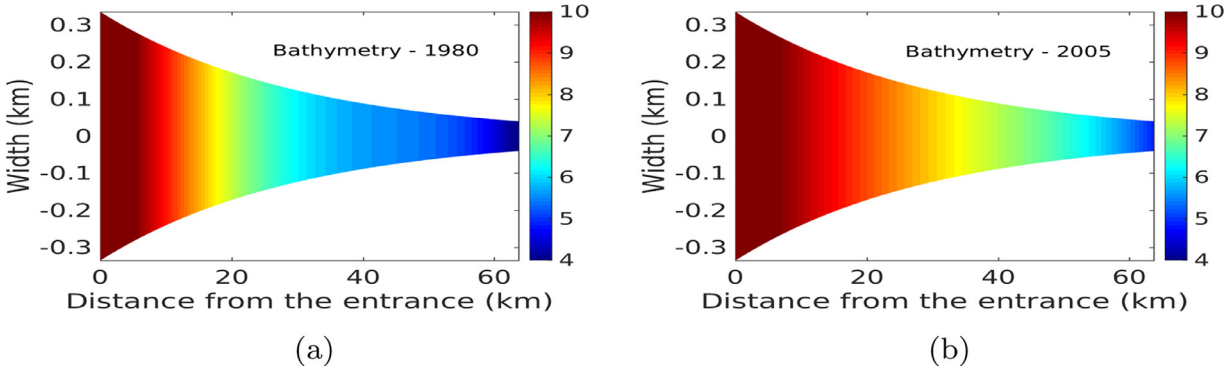

Fig. 4. Bathymetry of the Ems estuary for the years 1980 and 2005 assuming laterally uniform conditions. The units in the colourbar are m. (For interpretation of the references to colour in this figure legend, the reader is referred to the web version of this article.)

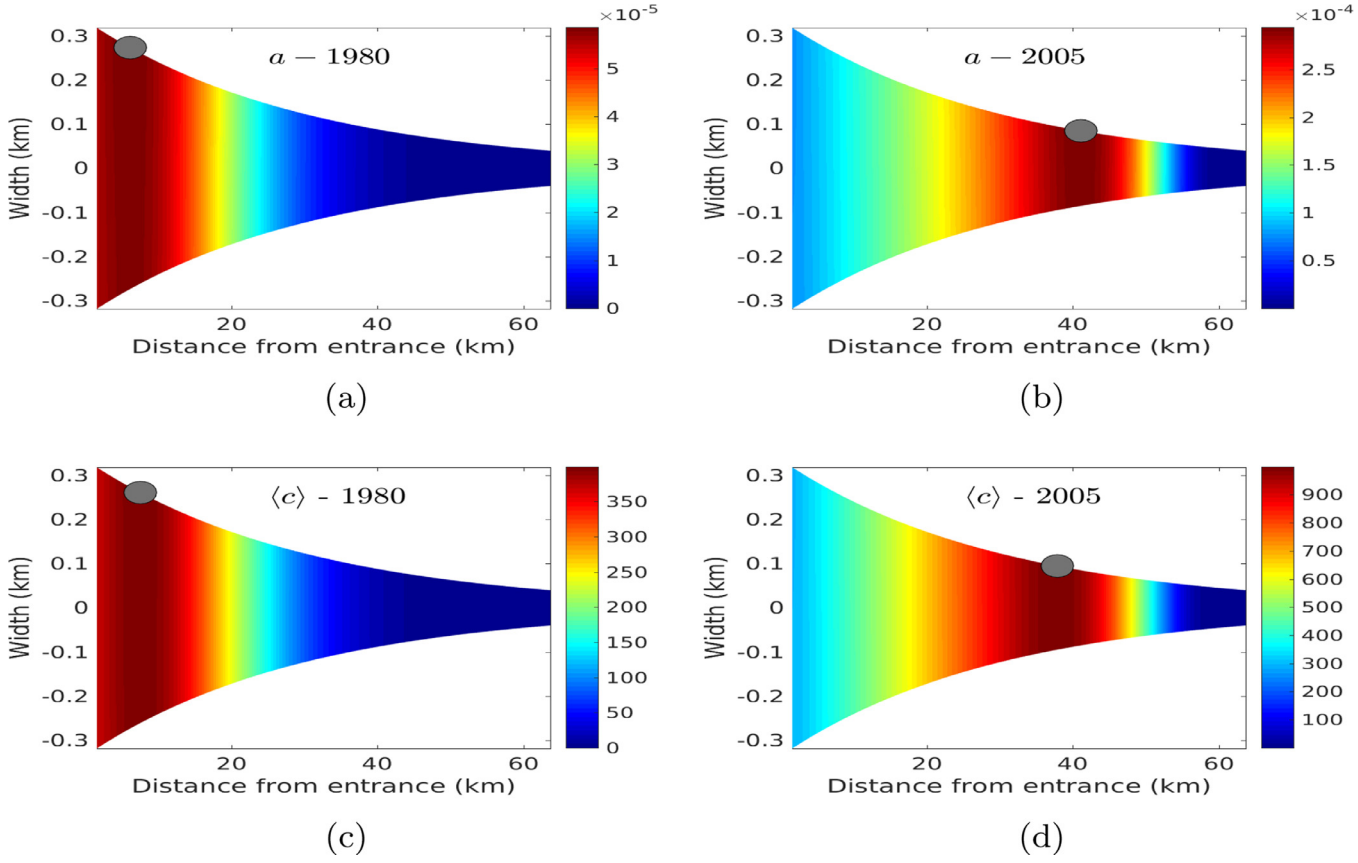

Fig. 5. Sediment availability (dimensionless) in the channel for the years 1980 (*top left*) and 2005 (*top right*). The tidally-averaged suspended sediment concentration at the surface for the years 1980 (*bottom left*) and 2005 (*bottom right*). The units in the colourbar are mg l^{-1}. The grey dots show the location of the maxima of the quantity being plotted. Note that the total amount of easily erodible sediment a_{total} is chosen in such a way that the maximum concentration at the surface for 1980 is 400 mg l^{-1} and for 2005 is 1000 mg l^{-1}. (For interpretation of the references to colour in this figure legend, the reader is referred to the web version of this article.)

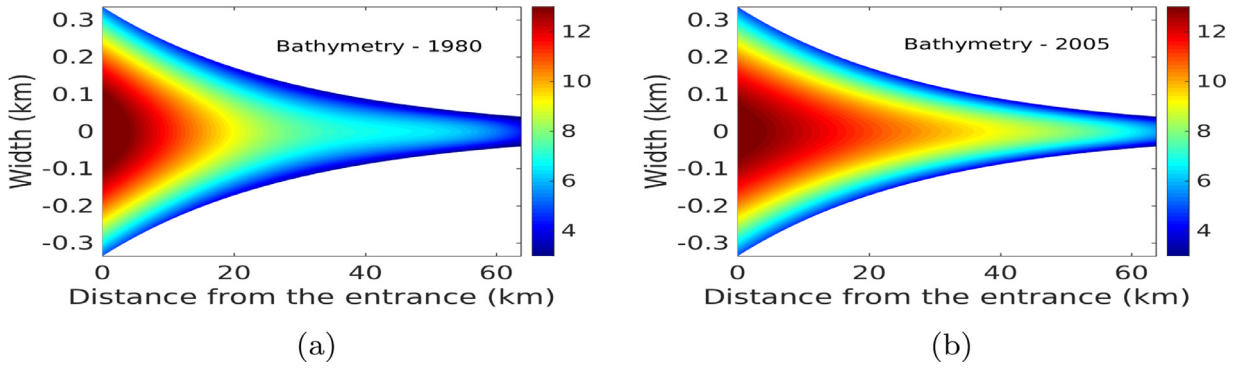

Fig. 6. The bathymetry of the Ems estuary for the years 1980 and 2005 varying parabolically in the lateral direction. The units in the colourbar are m. (For interpretation of the references to colour in this figure legend, the reader is referred to the web version of this article.)

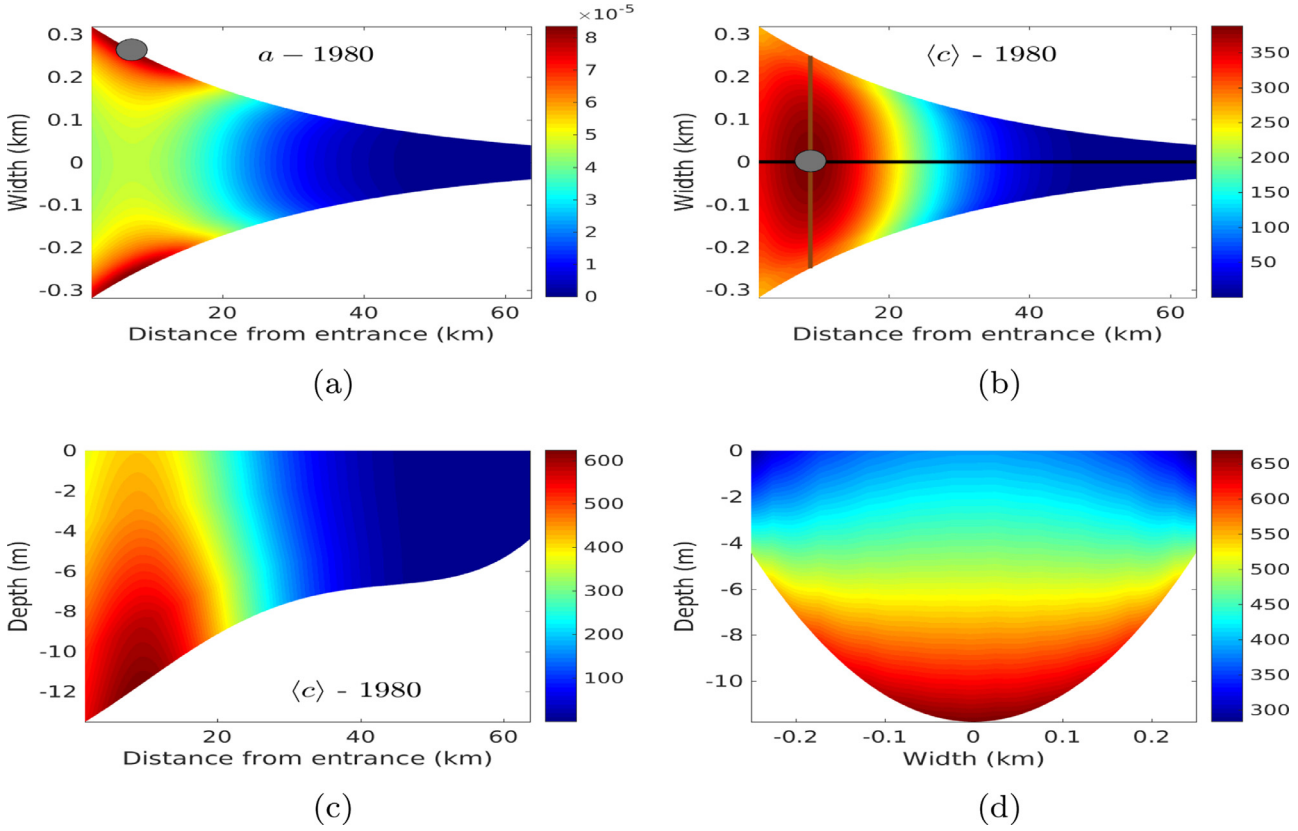

Fig. 7. Sediment availability and sediment concentration for 1980 with laterally varying bed profile. The *top left panel* shows the sediment availability (dimensionless) and *top right panel*, the sediment concentration (mg l^{-1}) at the surface. The black and chocolate lines pass through the location of maximum concentration at the surface in the x and y directions, respectively. The grey dot indicates the location of the maximum of the quantity being plotted. The *bottom left panel* shows the cross-sectional profile of the sediment concentration along the black line and the *bottom right panel*, along the chocolate line. (For interpretation of the references to colour in this figure legend, the reader is referred to the web version of this article.)

where $\boldsymbol{u}_{\mathrm{h}} = (u, v)$ denotes the horizontal velocity and $\hat{\mathbf{n}}$, the horizontal unit normal vector pointing outwards. The outer integral in Eq. (2b) denotes the line integral over the river boundary. Importantly, $-Q$ is the total inflow of fresh water over one river boundary. If there is more than one river inlet (shown in cyan colour in Fig. 2), appropriate river discharges Q are assigned to each one. Since we are focussing on tidally dominated systems, the river discharge is assumed to be small compared with the tidal discharge (see Section 3.5). At the closed boundaries ($\partial_C\Omega$), a no-transport condition is imposed,

$$\int_{-h}^{\eta} \boldsymbol{u}_{\mathrm{h}} \cdot \hat{\mathbf{n}}\, \mathrm{d}z = 0, \quad \text{for all } (x, y) \text{ in } \partial_C\Omega. \tag{2c}$$

It is not possible to require the flux to vanish at each point in the vertical at the boundary. This is a consequence of neglecting the horizontal viscous effects, by which the horizontal viscous boundary layer is not resolved. Following Winant (2007), this is acceptable since the thickness of this boundary layer is negligible compared with the horizontal length scale we are focusing on (length scale of the order of the length of the estuary).

At the free surface $z = \eta$, kinematic and dynamic boundary conditions are imposed,

$$w = \frac{\partial \eta}{\partial t} + u\frac{\partial \eta}{\partial x} + v\frac{\partial \eta}{\partial y}, \quad \text{at } z = \eta, \tag{2d}$$

$$A_v \frac{\partial \boldsymbol{u}_h}{\partial z} = \mathbf{0}_h, \quad \text{at } z = \eta, \tag{2e}$$

where $\mathbf{0}_h = (0, 0)$ is the two-dimensional horizontal null vector. At the bottom $z = -h$, the non-permeability condition (kinematic) and the dynamic boundary condition are prescribed,

$$w = -u\frac{\partial h}{\partial x} - v\frac{\partial h}{\partial y}, \quad \text{at } z = -h, \tag{2f}$$

$$A_v \frac{\partial \boldsymbol{u}_h}{\partial z} = \frac{\boldsymbol{\tau}_b}{\rho_0} = s\boldsymbol{u}_h, \quad \text{at } z = -h, \tag{2g}$$

where $s(x, y)$ is the so-called stress parameter which follows from the linearization of the bed shear stress (see Zimmerman, 1992). If $s \to 0$, this formulation reduces to the free-slip condition, for $s \to \infty$ to the no-slip condition. It is important to point out that by adopting this simplification, the constant stress layer near the bed where the viscosity goes to zero, is neglected, see Schramkowski et al. (2002) for details. Here, we have assumed that both the bottom slopes and the surface elevation slopes are much smaller than 1, i.e., $|\nabla h|, |\nabla \eta| \ll 1$.

3.3. Suspended sediment concentration

The suspended sediment concentration is modelled by a three-dimensional advection-diffusion equation

$$\frac{\partial c}{\partial t} + \nabla \cdot \mathbf{F} = 0, \tag{3}$$

with $\mathbf{F} = \mathbf{F}_a + \mathbf{F}_s + \mathbf{F}_d$, the sediment flux that consists of three different contributions: the advective flux $\mathbf{F}_a$, the settling flux $\mathbf{F}_s$ and the diffusive flux $\mathbf{F}_d$. These fluxes are given by

$$\mathbf{F}_a = c\boldsymbol{u},$$
$$\mathbf{F}_s = -(0, 0, cw_s),$$
$$\mathbf{F}_d = -\left(K_h\frac{\partial c}{\partial x}, K_h\frac{\partial c}{\partial y}, K_v\frac{\partial c}{\partial z}\right),$$

where w_s denotes the settling velocity, and $K_h(x, y)$ and $K_v(x, y)$ the horizontal and vertical diffusivities, respectively. The vertical diffusivity K_v is assumed to be equal to the vertical eddy viscosity A_v. Using these expressions, Eq. (3) becomes

$$\frac{\partial c}{\partial t} + \frac{\partial}{\partial x}\left(cu - K_h\frac{\partial c}{\partial x}\right) + \frac{\partial}{\partial y}\left(cv - K_h\frac{\partial c}{\partial y}\right) + \frac{\partial}{\partial z}\left(c(w - w_s) - K_v\frac{\partial c}{\partial z}\right) = 0. \tag{4}$$

At the free surface $z = \eta$ and the bottom $z = -h$, the outward normal component of the sum of the settling and diffusive fluxes is required to be equal to a specified erosion-deposition flux of volume concentration S_*, i.e.,

$$-(\mathbf{F}_s + \mathbf{F}_d) \cdot \hat{\mathbf{n}} = S_*, \tag{5}$$

where $\hat{\mathbf{n}}$ is the unit normal vector pointing outwards.

At the free surface, using $|\nabla \eta| \ll 1$, $\hat{\mathbf{n}} = (-\eta_x, -\eta_y, 1)$, and $S_* = 0$ results in

$$-K_h c_x \eta_x - K_h c_y \eta_y + w_s c + K_v c_z = 0 \quad \text{at } z = \eta. \tag{6a}$$

At the bottom, using $|\nabla h| \ll 1$, $\hat{\mathbf{n}} = (-h_x, -h_y, -1)$, and $S_* = E - D$, where $E = w_s c_{\text{ref}}$ is the erosion and $D = w_s c_0$, the deposition. Here c_{ref} is a reference concentration and c_0 is the actual concentration at the bottom, i.e., $c_0 = c|_{z=-h}$. The bottom boundary condition thus becomes

$$-K_h c_x h_x - K_h c_y h_y - K_v c_z = w_s c_{\text{ref}}, \quad \text{at } z = -h, \tag{6b}$$

with the reference concentration c_{ref} given as

$$c_{\text{ref}} = \frac{\rho_s a|\boldsymbol{\tau}_b|}{\rho_0 g' d_s}. \tag{6c}$$

Here $|\boldsymbol{\tau}_b|$ denotes the absolute value of the bed shear stress and $a(x, y)$ represents the availability of fine sediments at location (x, y). Note that $a(x, y)$ is a spatially varying coefficient parameterizing the ease with which fine sediments can be eroded and the amount of easily erodible fine sediments available at location (x, y) (Friedrichs et al., 1998; Chernetsky et al., 2010; Huijts et al., 2006). The sediment density is denoted by ρ_s, $g' = g(\rho_s - \rho)/\rho_0$ is the reduced gravity, and $d_s(x, y)$ is the grain size of the sediments.

It should be noted that in Eq. (4) the horizontal diffusivities are retained. However, to be consistent with the solution procedure for the hydrodynamic equations, the boundary layers for the suspended sediments will also not be resolved and the horizontal diffusivities will only play a role in the morphodynamic equilibrium condition (see Section 3.4) . Hence Eq. (4), together with the boundary conditions given by Eq. (6) complete the system of equations governing the suspended sediment concentration in the estuary for given availability $a(x, y)$.

3.4. Condition of morphodynamic equilibrium

We consider a state of the system in which tidally averaged erosion and deposition balance each other:

$$\langle D - E \rangle = 0, \tag{7}$$

where $\langle\cdot\rangle$ denotes a tidally-averaged quantity (see Van Rijn, 1993 for more details). This condition is termed as the morphodynamic equilibrium condition (Chernetsky et al., 2010; Huijts et al., 2006; Friedrichs et al., 1998).

Integrating the sediment concentration equation over the water column (from $z = -h$ to $z = \eta$) and using the boundary conditions for water motion and suspended sediment concentration at the free surface and at the bottom results in

$$\frac{\partial}{\partial t}\int_{-h}^{\eta} c\, \mathrm{d}z + \frac{\partial}{\partial x}\int_{-h}^{\eta}\left(cu - K_h\frac{\partial c}{\partial x}\right)\mathrm{d}z + \frac{\partial}{\partial y}\int_{-h}^{\eta}\left(cv - K_h\frac{\partial c}{\partial y}\right)\mathrm{d}z + D - E = 0.$$

Averaging the above equation over the tidal period, using Eq. (7), we find that the condition of morphodynamic equilibrium requires that

$$\left\langle \frac{\partial}{\partial x}\int_{-h}^{\eta}\left(cu - K_h\frac{\partial c}{\partial x}\right)\mathrm{d}z + \frac{\partial}{\partial y}\int_{-h}^{\eta}\left(cv - K_h\frac{\partial c}{\partial y}\right)\mathrm{d}z \right\rangle = 0. \tag{8}$$

This condition together with the requirement that there is no tidally averaged sediment transport through the boundaries, can only be satisfied if the easily erodible fine sediment has a specific spatial distribution, i.e., Eq. (8) is effectively a condition for $a(x, y)$.

3.5. Scaling and perturbation analyses

Next, the equations for the water motion, suspended sediment concentration and morphodynamic equilibrium are scaled by introducing dimensionless variables. This results in the identification of a small parameter ϵ defined as

$$\epsilon = \bar{A}_{M_2}/H \ll 1.$$

Here, $\bar{A}_{M_2}$ is the mean elevation amplitude of the M_2 tide at the seaward boundary and H the mean depth at the seaward boundary. The order of magnitude of all other dimensionless numbers is related to this parameter ϵ, thus indicating the relative importance

of each contribution. Next, the unknown physical variables are expanded in this small parameter (see Nayfeh, 2007 for details about perturbation methods). These asymptotic expansions are inserted in the dimensionless system of equations and terms of equal order in ϵ are collected. This results in systems of equations at each order in ϵ (see Appendix A for a detailed description of the scaling and perturbation analyses).

In the following sections, we present the systems of equations in their dimensional form and the solution procedure used to solve the leading-order (ϵ^0) and first-order (ϵ^1) system of equations for the water motion (Sections 4 and 5) and the suspended sediment concentration (Sections 6 and 7). Finally, the sediment availability $a(x, y)$ is obtained by solving the condition of morphodynamic equilibrium which is encountered only at second order (ϵ^2).

For clarification, let us now introduce the notation convention. In ϕ^{mn}, where ϕ is any of the unknown physical variables, i.e., $\phi = \{\eta, \boldsymbol{u}, c\}$, the first superscript m denotes the order in ϵ of that contribution and the second superscript n its tidal frequency. For example, η^{02} denotes the leading-order (ϵ^0) M_2 surface elevation and $\boldsymbol{u}^{14}$ denotes the first-order (ϵ^1) M_4 velocity vector.

4. Leading-order water motion

The leading-order system of equations for the water motion reads

$$u^0_x + v^0_y + w^0_z = 0, \tag{9a}$$

$$u^0_t - fv^0 = -g\eta^0_x + (A_v u^0_z)_z, \tag{9b}$$

$$v^0_t + fu^0 = -g\eta^0_y + (A_v v^0_z)_z, \tag{9c}$$

with boundary conditions at the free surface

$$\rho_0 A_v (\boldsymbol{u}^0_h)_z = \boldsymbol{0}_h, \quad \text{and} \quad w^0 = \eta^0_t, \quad \text{at} \quad z = 0.$$

Note that, as a result of the scaling procedure, this boundary condition is prescribed at $z = 0$ (see Appendix A for details). At the bottom $z = -h$, we require that

$$A_v(\boldsymbol{u}^0_h)_z = s\boldsymbol{u}^0_h, \quad \text{and} \quad w^0 = -u^0 h_x - v^0 h_y, \quad \text{at} \quad z = -h.$$

The water motion at leading-order is only forced by the M_2 tidal constituent at the seaward boundary,

$$\eta^0 = A_{M_2} \cos(\omega t - \phi_{M_2}) \quad \text{for all} \quad (x, y) \text{ in } \partial_S\Omega,$$

while the transport through the other boundaries vanishes

$$\int_{-h}^{0} \boldsymbol{u}^0_h \cdot \hat{\mathbf{n}} \, dz = 0, \quad \text{for all} \quad (x, y) \text{ in } \partial_R\Omega \text{ or } \partial_C\Omega.$$

As already pointed out in Section 3.2, it is assumed that the river inflow gives a contribution only at $\mathcal{O}(\epsilon)$ and hence does not appear in the leading order system of equations. The solution of this system of equations describes the propagation of a tidal wave in a homogeneous fluid (no density effects) in an estuary with an arbitrary geometry and bathymetry. Here, only a brief outline of the solution method is presented.

To solve the leading-order water motion (see Kumar et al., 2016 for details), we write

$$(\eta^0, \boldsymbol{u}^0) = \Re\{(N^{02}, \boldsymbol{U}^{02}) e^{i\omega t}\}, \tag{10}$$

where $\Re$ stands for the real part of a complex variable, and N^{02} and $\boldsymbol{U}^{02} = (U^{02}, V^{02}, W^{02})$ are spatially varying complex amplitudes of the surface elevation and the velocity field, respectively. The vertical structure of the leading-order velocity field can be obtained analytically using Eqs. (9b) and (9c); it is proportional to the first- and second-order partial derivatives of the leading-order surface elevation.

The surface elevation N^{02} and its partial derivatives are obtained by integrating the leading-order continuity equation (Eq. (9a)) over the water column. Using the appropriate boundary conditions, a two-dimensional elliptic partial differential equation for the leading-order surface elevation N^{02} is obtained. This equation is solved numerically using the finite element method (see Section 9 for details).

5. First-order water motion

The first-order system of equations for the water motion reads

$$u^1_x + v^1_y + w^1_z = 0, \tag{11a}$$

$$u^1_t + F^x_{AC} - fv^1 = -g\eta^1_x + F^x_{GC} + (A_v u^1_z)_z, \tag{11b}$$

$$v^1_t + F^y_{AC} + fu^1 = -g\eta^1_y + F^y_{GC} + (A_v v^1_z)_z, \tag{11c}$$

where $\{F^x_{AC}, F^y_{AC}\}$ denote the advective terms and $\{F^x_{GC}, F^y_{GC}\}$, the forcing due to density gradients. The different forcing terms are defined in Table 1. At the seaward boundary, an external M_4 tide (F_{EF}) is prescribed

$$\eta^1 = F_{EF}, \quad \text{for all} \quad (x, y) \text{ in } \partial_S\Omega. \tag{11d}$$

At the river boundary, a river discharge density Q' is prescribed, $F_{RD} = -Q'$,

$$\int_{-h}^{0} \boldsymbol{u}^1_h \cdot \hat{\mathbf{n}} \, dz + F^{\partial\Omega}_{TRF} = F_{RD}, \quad \text{for all} \quad (x, y) \text{ in } \partial_R\Omega. \tag{11e}$$

The total river discharge Q is distributed over the river boundary by requiring that

$$\int_{\partial_R\Omega} Q' \, ds = Q. \tag{11f}$$

The contribution $F^{\partial\Omega}_{TRF}$ is the transport through the boundary due to the correlation between the leading-order surface elevation and the velocity. At the closed boundary $\partial_C\Omega$, the total transport must vanish which implies that the first-order transport must balance the transport due to the correlation between the leading-order surface elevation and the velocity,

$$\int_{-h}^{0} \boldsymbol{u}^1_h \cdot \hat{\mathbf{n}} \, dz + F^{\partial\Omega}_{TRF} = 0, \quad \text{for all} \quad (x, y) \text{ in } \partial_C\Omega. \tag{11g}$$

At the free surface, the first-order stress must balance the stress due to the leading-order solution, denoted by F_{NS}, evaluated at $z = 0$.

$$\rho_0 A_v (\boldsymbol{u}^1_h)_z = -F_{NS}, \quad \text{at} \quad z = 0. \tag{11h}$$

The forcing in the interior due to the correlation between the leading-order surface elevation and velocity, denoted by F^{Ω}_{TRF}, appears in the kinematic boundary condition as

$$w^1 = \eta^1_t + F^{\Omega}_{TRF}, \quad \text{at} \quad z = 0. \tag{11i}$$

For the boundary conditions at the bottom, no new forcing terms are obtained, i.e.,

$$A_v(\boldsymbol{u}^1_h)_z = s\boldsymbol{u}^1_h, \quad \text{and} \quad w^1 = -u^1 h_x - v^1 h_y, \quad \text{at} \quad z = -h. \tag{11j}$$

Since the leading-order flow is known, the system of equations for the first-order water motion and its boundary conditions are linear in the unknown surface elevation η^1 and velocity field $\boldsymbol{u}^1 = (u^1, v^1, w^1)$. As a result, this equation can be solved for each forcing term F individually.

Table 1
Various forcing terms appearing in the first-order system of equations for the water motion (Eq. (11)). The value of n denotes the frequency M_n of the forcing terms.

Name	Mathematical expression	Abbreviation	n
Externally prescribed			
Gravitational circulation	$\frac{g}{\rho_0} z(\rho_x, \rho_y)$	(F^x_{GC}, F^y_{GC})	0
External M_4	$A_{M_4}\cos(2\omega t - \phi_{M_4})$	F_{EF}	4
River discharge	$-Q'$	F_{RD}	0
Internally generated			
Advection	$u^{02}(\boldsymbol{u}^{02}_{\mathrm{h}})_x + v^{02}(\boldsymbol{u}^{02}_{\mathrm{h}})_y + w^{02}(\boldsymbol{u}^{02}_{\mathrm{h}})_z$	(F^x_{AC}, F^y_{AC})	0,4
No-stress	$\rho_0 A_v \eta^{02} u^{02}_{zz}\|_{z=0}$	F_{NS}	0,4
Tidal return flow	$\nabla\cdot(\eta^0 \boldsymbol{u}^{02}_{\mathrm{h}})\|_{z=0}$	F^{Ω}_{TRF}	0,4
	$(\eta^{02}\boldsymbol{u}^{02}_{\mathrm{h}})\cdot\hat{\mathbf{n}}\|_{\partial_R\Omega\cup\partial_C\Omega}$	$F^{\partial\Omega}_{TRF}$	

The forcing terms F can be divided into two categories: *externally prescribed* and *internally generated*. Table 1 gives a full list of all forcing terms for the first-order water motion. The externally prescribed forcing terms are those prescribed explicitly, e.g., the external M_4 tide, time-independent river discharge and density gradients. The internally generated forcing terms are generated by the non-linear interaction of the leading-order flow variables (advection, no-stress and tidal return flow). It is important to note that the forcing terms due to the non-linear interactions of leading-order water motion are either time-independent or are forcing terms with an M_4 periodicity. Therefore, both externally prescribed and internally generated forcing terms can be written as

$$F = \Re\{F^{1n} e^{\frac{ni\omega t}{2}}\}, \tag{12}$$

where $n = 0$ or 4 depending on the forcing term (see Table 1 for values of n). This allows us to write the solution of the first-order water motion as

$$(\eta^{1n}, \boldsymbol{u}^{1n}) = \Re\{(N^{1n}, \boldsymbol{U}^{1n}) e^{\frac{ni\omega t}{2}}\},$$

where the terms with the superscript 10 ($n = 0$) denote first-order M_0 components and those with a superscript 14 ($n = 4$), first-order M_4 components. Here N^{1n} and $\boldsymbol{U}^{1n} = (U^{1n}, V^{1n}, W^{1n})$ are the spatially varying complex amplitudes of the first-order surface elevation and velocity field, respectively. The first-order system for nth tidal frequency thus becomes

$$U^{1n}_x + V^{1n}_y + W^{1n}_z = 0, \tag{13a}$$

$$\frac{ni\omega}{2} U^{1n} + F^{x,1n}_{AC} - fV^{1n} = -gN^{1n}_x + F^{x,10}_{GC} + (A_v U^{1n}_z)_z, \tag{13b}$$

$$\frac{ni\omega}{2} V^{1n} + F^{y,1n}_{AC} + fU^{1n} = -gN^{1n}_y + F^{y,10}_{GC} + (A_v V^{1n}_z)_z. \tag{13c}$$

In a similar way, the boundary conditions can be expressed in terms of the complex amplitudes. This introduces new terms $F^{\Omega,1n}_{TRF}$ and $F^{\partial\Omega,1n}_{TRF}$ which denote the nth frequency component of F^{Ω}_{TRF} and $F^{\partial\Omega}_{TRF}$, respectively.

To solve for the complex amplitudes N^{1n} and $\boldsymbol{U}^{1n}$, rotating flow variables are introduced:

$$r^{1n}_1 = U^{1n} + iV^{1n}, \quad \text{and} \quad r^{1n}_2 = U^{1n} - iV^{1n}. \tag{14}$$

Combining Eqs. (13b) and (13c), the equations for the rotating flow variables r^{1n}_1 and r^{2n}_2 are obtained:

$$r^{1n}_{j,zz} - (\alpha^n_j)^2 r^{1n}_j = \frac{g}{A_v}\mathcal{L}_j N^{1n} + F^{1n}_{AC,j} + F^{10}_{GC,j}, \quad \text{for } j = 1, 2, \tag{15a}$$

together with the boundary conditions

$$\rho_0 A_v r^{1n}_{j,z} = F^{1n}_{NS,j}, \quad \text{at } z = 0, \tag{15b}$$

$$\rho_0 A_v r^{1n}_{j,z} = \rho_0 s r^{1n}_j, \quad \text{at } z = -h. \tag{15c}$$

Table 2
Forcing terms appearing in the equations for rotating variables.

Notation	Definition
$(F^{10}_{GC,1}, F^{10}_{GC,2})$	$-\frac{1}{A_v}(F^{x,10}_{GC} \pm iF^{y,10}_{GC})$
$(F^{1n}_{AC,1}, F^{1n}_{AC,2})$	$\frac{1}{A_v}(F^{x,1n}_{AC} \pm iF^{y,1n}_{AC})$
$(F^{1n}_{NS,1}, F^{1n}_{NS,2})$	$F^{x,1n}_{NS} \pm iF^{y,1n}_{NS}$

In Eq. (15a), the operators $\mathcal{L}_j$ are defined by $\mathcal{L}_1 = \partial_x + i\partial_y$, and $\mathcal{L}_2 = \partial_x - i\partial_y$, and α^n_j by

$$\alpha^n_1 = \sqrt{i\frac{n\omega + 2f}{2A_v}}, \quad \text{and} \quad \alpha^n_2 = \sqrt{i\frac{n\omega - 2f}{2A_v}}, \quad n = 0, 4.$$

For $n = 4$, α^n_1 and α^n_2 are related to the cyclonic and anticyclonic boundary layer thickness $\delta_\pm = \sqrt{\frac{2A_v}{n\omega/2 \pm f}}$ associated with the M_4 tidal constituent (Soulsby, 1983; Souza, 2013). Similarly, for $n = 0$, the parameters are related to the time-independent boundary layer thickness. The forcing terms in the equations for rotating variables are linear combinations of the forcing terms in the original equations; see Table 2.

The equations for the rotating flow variables can be solved analytically,

$$r^{1n}_j(x, y, z) = c_{\alpha^n_j}(x, y, z)\mathcal{L}_j N^{1n} + f_{\alpha^n_j}(x, y, z), \quad j = 1, 2,$$

with

$$c_{\alpha^n_j}(x, y, z) = \frac{g}{(\alpha^n_j)^2 A_v}\left[\frac{s\cosh(\alpha^n_j z)}{\alpha^n_j A_v \sinh(\alpha^n_j h) + s\cosh(\alpha^n_j h)} - 1\right].$$

Expressions for $f_{\alpha^n_j}$ depend on the forcing term under consideration. Integrating these expressions over the depth gives

$$\int_{-h}^{0} r^n_j(x, y, z')\, \mathrm{d}z' = C_{\alpha^n_j}(x, y)\mathcal{L}_j N^{1n} + F_{\alpha^n_j}(x, y), \quad j = 1, 2,$$

where

$$C_{\alpha^n_j}(x, y) = \frac{g}{(\alpha^n_j)^3 A_v}\left[\frac{s\sinh(\alpha^n_j h)}{\alpha^n_j A_v \sinh(\alpha^n_j h) + s\cosh(\alpha^n_j h)} - \alpha^n_j h\right].$$

Using Eq. (14), the depth-dependent and depth-integrated horizontal velocities can be obtained in terms of the gradients of the surface elevation and known forcing terms as

$$(U^{1n}, V^{1n}) = (d_1, -d_2)N^{1n}_x + (d_2, d_1)N^{1n}_y + (f^{1n}_1, f^{1n}_2), \tag{16}$$

$$\int_{-h}^{0} (U^{1n}, V^{1n})\, \mathrm{d}z = (D_1, -D_2)N^{1n}_x + (D_2, D_1)N^{1n}_y + (F^{1n}_1, F^{1n}_2), \tag{17}$$

where

$$(d^{1n}_1, f^{1n}_1, D^{1n}_1, F^{1n}_1)$$

$$= \frac{1}{2}\left[(c_{\alpha_1^n}, f_{\alpha_1^n}, C_{\alpha_1^n}, F_{\alpha_1^n}) + (c_{\alpha_2^n}, f_{\alpha_2^n}, C_{\alpha_2^n}, F_{\alpha_2^n})\right],$$

$$(d_2^{1n}, f_2^{1n}, D_2^{1n}, F_2^{1n})$$

$$= \frac{i}{2}\left[(c_{\alpha_1^n}, -f_{\alpha_1^n}, C_{\alpha_1^n}, -F_{\alpha_1^n}) - (c_{\alpha_2^n}, -f_{\alpha_2^n}, C_{\alpha_2^n}, -F_{\alpha_2^n})\right].$$

To obtain the surface elevation, the first-order continuity equation is integrated over the water column (from $z = -h$ to $z = 0$). Together with the boundary conditions at $z = -h$ and $z = 0$, this gives

$$\frac{\partial}{\partial x}\int_{-h}^{0} U^{1n}\,\mathrm{d}z + \frac{\partial}{\partial y}\int_{-h}^{0} V^{1n}\,\mathrm{d}z + \frac{ni\omega}{2}N^{1n} + F_{TRF}^{\Omega,1n} = 0.$$

Inserting the expressions for depth-integrated horizontal velocity given by Eq. (16) in the above equation gives a second-order elliptic partial differential equation for the surface elevation N^{1n}

$$\nabla\cdot\left(\mathbf{D}^{1n}\nabla N^{1n} + \mathbf{F}^{1n}\right) + \frac{ni\omega}{2}N^{1n} + F_{TRF}^{\Omega,1n} = 0, \tag{18a}$$

where

$$\mathbf{D}^{1n} = \begin{pmatrix} D_1^{1n} & D_2^{1n} \\ -D_2^{1n} & D_1^{1n} \end{pmatrix}, \text{ and } \mathbf{F}^{1n} = \begin{pmatrix} F_1^{1n} \\ F_2^{1n} \end{pmatrix}.$$

The associated horizontal boundary conditions read:

$$N^{1n} = F_{EF}^{14}, \text{ for all } (x, y) \text{ in } \partial_S\Omega, \tag{18b}$$

$$(\mathbf{D}^{1n}\nabla N^{1n} + \mathbf{F}^{1n})\cdot\hat{\mathbf{n}} + F_{TRF}^{\partial\Omega,1n} = F_{RD}^{10}, \text{ for all } (x, y) \text{ in } \partial_R\Omega, \tag{18c}$$

$$(\mathbf{D}^{1n}\nabla N^{1n} + \mathbf{F}^{1n})\cdot\hat{\mathbf{n}} + F_{TRF}^{\partial\Omega,1n} = 0, \text{ for all } (x, y) \text{ in } \partial_C\Omega. \tag{18d}$$

Since this equation for the surface elevation is a linear equation, it can be solved for each forcing term separately (i.e., each forcing term is studied individually by putting all other forcing terms to zero), thus resulting in explicit expressions for the first-order velocity due to each forcing term separately. The elliptic equation for N^{1n} has to be solved numerically, for details see Section 9.

The first-order horizontal velocity $\boldsymbol{u}_{\mathrm{h}}^1$ can be written as sum of M_0 and M_4 tidal constituents,

$$\boldsymbol{u}_{\mathrm{h}}^1 = \boldsymbol{u}_{\mathrm{h}}^{10} + \boldsymbol{u}_{\mathrm{h}}^{14}, \tag{19a}$$

which can be further expressed as a sum of various constituents of the first-order water motion, i.e.,

$$\boldsymbol{u}_{\mathrm{h}}^{10} = \boldsymbol{u}_{\mathrm{h},GC}^{10} + \boldsymbol{u}_{\mathrm{h},RD}^{10} + \boldsymbol{u}_{\mathrm{h},AC}^{10} + \boldsymbol{u}_{\mathrm{h},NS}^{10} + \boldsymbol{u}_{\mathrm{h},TRF}^{10}, \tag{19b}$$

$$\boldsymbol{u}_{\mathrm{h}}^{14} = \boldsymbol{u}_{\mathrm{h},EF}^{14} + \boldsymbol{u}_{\mathrm{h},AC}^{14} + \boldsymbol{u}_{\mathrm{h},NS}^{14} + \boldsymbol{u}_{\mathrm{h},TRF}^{14}. \tag{19c}$$

See Table 1 for an explanation of abbreviations in Eq. (19). The first-order vertical velocity W^{1n} can be obtained by integrating the first-order continuity equation in the vertical direction from $z' = -h$ to $z' = z$ (see Kumar et al., 2016 for a detailed explanation).

6. Leading-order suspended sediment concentration

The leading-order equation for the suspended sediment concentration is given by

$$c_t^0 - (K_{\mathrm{v}}c_z^0)_z - (w_{\mathrm{s}}c^0)_z = 0. \tag{20a}$$

The boundary condition at the free surface reads

$$K_{\mathrm{v}}c_z^0 + w_{\mathrm{s}}c^0 = 0, \text{ at } z = 0, \tag{20b}$$

and at the bottom

$$K_{\mathrm{v}}c_z^0 + a\frac{w_{\mathrm{s}}\rho_{\mathrm{s}}}{\rho_0 g' d_{\mathrm{s}}}|\boldsymbol{\tau}_b|^0 = 0, \text{ at } z = -h. \tag{20c}$$

Here $|\boldsymbol{\tau}_b|^0$ denotes the leading-order component of the absolute value of the bed shear stress. From Eq. (20), it follows that the leading-order suspended sediment concentration is solely driven by $|\boldsymbol{\tau}_b|^0$. Since the bed shear stress is written as the sum of a residual component and components with frequencies that are even multiples of the M_2 frequency, the leading-order suspended sediment concentration can also be written as

$$c^0 = c^{00} + c^{04} + \ldots$$

Even though Eq. (20) can be solved for any tidal constituent, only c^{00} and c^{04} are required to compute the leading-order residual transport (see Appendix B). To stress that the suspended sediment concentrations are linear in the unknown sediment availability $a(x, y)$, we can write

$$c^0 = a\tilde{c}^{0a} = a\tilde{c}^{00a} + a\tilde{c}^{04a} + \ldots \tag{21}$$

Here, $\tilde{c}^{00a}$, $\tilde{c}^{04a}$ and $\tilde{c}^{0a}$ are the M_0, M_4 and total leading-order suspended sediment concentrations obtained with $a = 1$. The superscript a indicates that these concentrations are proportional to a.

7. First-order suspended sediment concentration

The equation for the first-order suspended sediment concentrationc^1 is given by

$$c_t^1 + F_{AC}^c - (K_{\mathrm{v}}c_z^1)_z - (w_{\mathrm{s}}c^1)_z = 0, \tag{22a}$$

where $F_{AC}^c = u^0c_x^0 + v^0c_y^0 + w^0c_z^0$ expresses advection of the leading-order concentration by the leading-order velocity. At the surface, the first-order boundary condition reads

$$w_{\mathrm{s}}c^1 + K_{\mathrm{v}}c_z^1 = F_S^c, \text{ at } z = 0, \tag{22b}$$

where $F_S^c = -\eta_0\left[w_{\mathrm{s}}c_z^0 + K_{\mathrm{v}}c_{zz}^0\right]$ is the first-order correction to the balance between the leading-order settling and deposition fluxes (due to the fact that this flux is calculated at $z = 0$, instead of $z = \eta$, see also Appendix A). At the bottom, the boundary condition reads

$$K_{\mathrm{v}}c_z^1 + a\frac{w_{\mathrm{s}}\rho_{\mathrm{s}}}{\rho_0 g' d_{\mathrm{s}}}|\boldsymbol{\tau}_b|^1 = 0, \text{ at } z = -h. \tag{22c}$$

Here $|\boldsymbol{\tau}_b|^1$ denotes the first-order component of the absolute value of the bed shear stress.

The first-order suspended sediment concentration is the result of three different forcing terms, the advection of the leading-order concentration by the leading-order velocity (F_{AC}^c), the surface contribution (F_S^c) and the first-order bed shear stress (F_{BS}^c). Since the equation is linear, the resulting first-order concentration can be solved for each forcing individually.

At this point, it is important to remember that our aim is to get the main contributions to the first-order residual sediment transport (see Section 2). The only first-order residual sediment transport that depends on the first-order suspended sediment concentration c^1, is due to the tidally-averaged advection of c^1 by the leading-order velocities $\mathbf{u}^0$. Since the leading-order velocity only consists of an M_2 tidal constituent, only the M_2 constituent of the first-order suspended sediment concentration c^1 has to be calculated to get the residual suspended sediment transport due to the first-order suspended sediment concentrations. (see Sections 2 and 8). Therefore, in the following only the construction of the M_2 first order concentration will be discussed in detail.

7.1. Contribution due to advection

The equation governing the first-order suspended sediment concentration, resulting from the interaction of leading-order velocity and concentration, is given by

$$c^1_{AC,t} + F^c_{AC} - (K_v c^1_{AC,z})_z - (w_s c^1_{AC})_z = 0, \tag{23a}$$

with homogeneous boundary conditions

$$w_s c^1_{AC} + K_v c^1_{AC,z} = 0, \quad \text{at } z = 0, \tag{23b}$$

$$K_v c^1_{AC,z} = 0, \quad \text{at } z = -h. \tag{23c}$$

Since F^c_{AC} contains the gradients of the leading-order suspended sediment concentration, using Eq. (21), F^c_{AC} can be written as a sum of contributions proportional to a, a_x and a_y, i.e.,

$$F^c_{AC} = aF^a_{AC} + a_x F^{a_x}_{AC} + a_y F^{a_y}_{AC}, \tag{24}$$

where $F^a_{AC} = \tilde{c}^{0a}_x u^0 + \tilde{c}^{0a}_y v^0 + \tilde{c}^{0a}_z w^0$, $F^{a_x}_{AC} = \tilde{c}^{0a} u^0$, and $F^{a_y}_{AC} = \tilde{c}^{0a} v^0$. Since the leading-order flow consists only of an M_2 tidal constituent, we only need the M_0 and M_4 tidal constituents of the leading-order concentration c^0 to get the M_2 tidal component of F^c_{AC}.

Denoting the M_2 solution of c^1_{AC} as c^{12}_{AC}, we find that (see Appendix B for details)

$$c^{12}_{AC} = a\tilde{c}^{12a}_{AC} + a_x \tilde{c}^{12a_x}_{AC} + a_y \tilde{c}^{12a_y}_{AC}, \tag{25}$$

where $\tilde{c}^{12a}_{AC}$, $\tilde{c}^{12a_x}_{AC}$, and $\tilde{c}^{12a_y}_{AC}$ are the solutions proportional to a, a_x and a_y, respectively.

7.2. Contribution due to first-order bed shear stress

Analogous to the case of leading-order suspended sediment concentration, the first-order component of the absolute value of the bed sear stress $|\boldsymbol{\tau}_b|^1$ can be decomposed in a Fourier series using frequencies that are multiples of the M_2 tidal frequency. To get the dominant residual transport component, we are only interested in the M_2 component $|\boldsymbol{\tau}_b|^{12}$ of the first-order component of the absolute value of the bed shear stress $|\boldsymbol{\tau}_b|^1$.

The resulting suspended sediment concentration c^{12}_{BS} follows from the equation,

$$c^{12}_{BS,t} - (K_v c^{12}_{BS,z})_z - (w_s c^{12}_{BS})_z = 0,$$

with the boundary conditions,

$$w_s c^{12}_{BS} + K_v c^{12}_{BS,z} = 0, \quad \text{at } z = 0,$$

$$K_v c^{12}_{BS,z} + a\frac{w_s \rho_s}{\rho_0 g' d_s}|\boldsymbol{\tau}_b|^{12} = 0, \quad \text{at } z = -h,$$

where $|\boldsymbol{\tau}_b|^{12}$ denotes the M_2 component of $|\boldsymbol{\tau}_b|^1$. Similar to the leading-order suspended sediment concentration, we can define

$$c^{12}_{BS} = a\tilde{c}^{12a}_{BS}.$$

Note that $|\boldsymbol{\tau}_b|^{12}$ depends on the first-order velocity which itself is a sum of various contributions, for each of which we can compute the resulting suspended sediment concentration c^{12}_{BS}. In Table 3, a list of all these components is given.

7.3. Contribution due to forcing at the surface

The last contribution is the result of the inhomogeneous contribution in the boundary condition at the surface (Eq. 22b). Using the leading-order concentration equation, we can rewrite this surface boundary condition as

$$F^c_S = -\eta^0\left[w_s c^0_z + K_v c^0_{zz}\right] = -\eta^0 c^0_t,$$

Table 3
Various components of the first-order velocity (*first column*) and (corresponding) first-order concentration due to the bed shear stress (*second column*).

u^1_h	u^1_h components	c^{12}_{BS} components
$\boldsymbol{u}^{10}_h$	$\boldsymbol{u}^{10}_{h,GC}$	$c^{12}_{BS,GC}$
	$\boldsymbol{u}^{10}_{h,RD}$	$c^{12}_{BS,RD}$
	$\boldsymbol{u}^{10}_{h,AC}$	$c^{12}_{BS,AC10}$
	$\boldsymbol{u}^{10}_{h,NS}$	$c^{12}_{BS,NS10}$
	$\boldsymbol{u}^{10}_{h,TRF}$	$c^{12}_{BS,TRF10}$
$\boldsymbol{u}^{14}_h$	$\boldsymbol{u}^{10}_{h,EF}$	$c^{12}_{BS,EF}$
	$\boldsymbol{u}^{14}_{h,AC}$	$c^{12}_{BS,AC14}$
	$\boldsymbol{u}^{14}_{h,NS}$	$c^{12}_{BS,NS14}$
	$\boldsymbol{u}^{14}_{h,TRF}$	$c^{12}_{BS,TRF14}$

$$= -\eta^{02} c^{04}_t,$$
$$= -a\eta^{02}\tilde{c}^{04a}_t.$$

This inhomogeneous term $\eta^0 c^{04}$ results in both M_2 and M_6 contributions. The resulting solution for the M_2 component of the first-order suspended sediment concentration due to the surface forcing can be written as,

$$c^{12}_S = a\tilde{c}^{12a}_S.$$

7.4. Summary of the first-order concentration

The M_2 constituent of the first-order suspended sediment concentration is a sum of three components,

$$\begin{aligned} c^{12} &= c^{12}_{AC} + c^{12}_{BS} + c^{12}_S \\ &= a\underbrace{(\tilde{c}^{12a}_{AC} + \tilde{c}^{12a}_{BS} + \tilde{c}^{12a}_S)}_{\tilde{c}^{12a}} + a_x \underbrace{\tilde{c}^{12a_x}_{AC}}_{\tilde{c}^{12a_x}} + a_y \underbrace{\tilde{c}^{12a_y}_{AC}}_{\tilde{c}^{12a_y}} \\ &= a\tilde{c}^{12a} + a_x\tilde{c}^{12a_x} + a_y\tilde{c}^{12a_y}. \end{aligned}$$

It means that the first-order suspended sediment concentration consists of parts proportional to a, a_x and a_y. It is important to note that proportionality of the suspended sediment concentration to a_x and a_y is solely due to the advective component.

8. Condition of morphodynamic equilibrium

The leading-order morphodynamic equilibrium follows from inserting the asymptotic expansions of the horizontal velocities and concentrations in Eq. (8) and reads

$$\nabla \cdot (\mathbf{D}^a \nabla a + a\mathbf{T}) = 0, \tag{26a}$$

where

$$\mathbf{D}^a = \begin{pmatrix} D_{K_h} + T^{xa_x}_{M_2} & T^{xa_y}_{M_2} \\ T^{ya_x}_{M_2} & D_{K_h} + T^{ya_y}_{M_2} \end{pmatrix}, \quad \text{and} \quad \mathbf{T} = \begin{pmatrix} T^{xa} \\ T^{ya} \end{pmatrix}.$$

Here D_{K_h} is the contribution due to the horizontal diffusivity and the terms $T^{xa_x}_{M_2}$, $T^{xa_y}_{M_2}$, $T^{ya_x}_{M_2}$, and $T^{ya_y}_{M_2}$ are generated by the interaction of M_2 velocity and M_2 advective concentration.

T^{xa} and T^{ya} denote the leading-order tidally-averaged sediment transport in the x and y directions, respectively. The transport T^{xa} is a sum of various terms (see Appendix C for detailed expressions)

$$T^{xa} = T^{xa}_{M_0} + T^{xa}_{M_2} + T^{xa}_{M_4} + T^{xa}_{\text{surface}} + T^{xa}_{\text{diff}}, \tag{26b}$$

where $T^{xa}_{M_0}$ denotes the transport due to the interaction of the M_0 velocity and M_0 concentration. Remember that the M_0 velocity itself consists of various contributions (Table 3), for each of

Table 4
Decomposition of various transport terms $T^{xa}_{M_0}$, $T^{xa}_{M_2}$, and $T^{xa}_{M_4}$ into subcomponents. A similar decomposition can be made for the transport terms in the lateral direction.

Velocity		Concentration		Transport
$T^{xa}_{M_0}$				
u^{10}	u^{10}_{GC}	$\tilde{c}^{00}$		$T^{xa}_{M_0,GC}$
	u^{10}_{RD}			$T^{xa}_{M_0,RD}$
	u^{10}_{AC}			$T^{xa}_{M_0,AC}$
	u^{10}_{NS}			$T^{xa}_{M_0,NS}$
	u^{10}_{TRF}			$T^{xa}_{M_0,TRF}$
$T^{xa}_{M_2}$				
u^{02}		$\tilde{c}^{12}_{AC}$		$T^{xa}_{M_2,AC}$
		$\tilde{c}^{12}_{S}$		$T^{xa}_{M_2,S}$
		$\tilde{c}^{12}_{BS}$	$\tilde{c}^{12}_{BS,GC}$	$T^{xa}_{M_2,BS,GC}$
			$\tilde{c}^{12}_{BS,RD}$	$T^{xa}_{M_2,BS,RD}$
			$\tilde{c}^{12}_{BS,AC10}$	$T^{xa}_{M_2,BS,AC10}$
			$\tilde{c}^{12}_{BS,NS10}$	$T^{xa}_{M_2,BS,NS10}$
			$\tilde{c}^{12}_{BS,TRF10}$	$T^{xa}_{M_2,BS,TRF10}$
			$\tilde{c}^{12}_{BS,EF}$	$T^{xa}_{M_2,BS,EF}$
			$\tilde{c}^{12}_{BS,AC14}$	$T^{xa}_{M_2,BS,AC14}$
			$\tilde{c}^{12}_{BS,NS14}$	$T^{xa}_{M_2,BS,NS14}$
			$\tilde{c}^{12}_{BS,TRF14}$	$T^{xa}_{M_2,BS,TRF14}$
$T^{xa}_{M_4}$				
u^{14}	u^{14}_{EF}	$\tilde{c}^{04}$		$T^{xa}_{M_4,EF}$
	u^{14}_{AC}			$T^{xa}_{M_4,AC}$
	u^{14}_{NS}			$T^{xa}_{M_4,NS}$
	u^{14}_{TRF}			$T^{xa}_{M_4,TRF}$

which we can compute $T^{xa}_{M_0}$ (see Table 4 for a full list of all subcomponents). $T^{xa}_{M_2}$ is the transport due to the correlation between the M_2 velocity and M_2 concentration. Again, the M_2 concentration consists of various contributions (Table 3), implying that $T^{xa}_{M_2}$ can be computed for each contribution. Similarly, $T^{xa}_{M_4}$ is generated by the interaction of M_4 velocity and M_4 concentration. Once again, the M_4 velocity is a sum of various components as listed in Table 4 which allows us to decompose it into further subcomponents. Table 4 lists all the subcomponents of $T^{xa}_{M_0}$, $T^{xa}_{M_2}$, and $T^{xa}_{M_4}$. The component T^{xa}_{surface} is the transport due to the interaction of M_2 surface elevation, M_2 velocity and the leading-order concentration at the surface and T^{xa}_{diff} is the diffusive transport (see Appendix C for expressions). A similar decomposition can be made for the transport in the y-direction T^{ya}.

To solve Eq. (26a) for the sediment availability, we require that the transport vanishes at the boundary,

$$(\mathbf{D}^a \nabla a + a\mathbf{T}) \cdot \hat{\mathbf{n}} = 0, \quad \text{on } \partial_S\Omega \cup \partial_R\Omega \cup \partial_C\Omega. \tag{26c}$$

The equation for sediment availability a together with the no-transport condition (Neumann type boundary condition) above does not give a unique solution for the sediment availability a. Therefore, an extra condition is imposed, namely the total amount of sediment available for erosion a_{total} in the estuary is prescribed,

$$\iint_\Omega a \, \mathrm{d}\Omega = a_{\text{total}}. \tag{26d}$$

Eq. 26 has to be solved numerically for general domains. Here, we use the finite element method which is described in the next section.

9. Numerical solution

In Sections 4 and 5, it was shown that the leading-order and first-order water motion could be expressed in terms of the gradients of the surface elevation. The surface elevation itself follows from a two-dimensional elliptic partial differential equation. Similarly, the sediment availability (Section 8) follows from an elliptic differential equation (Eq. (26a)). Since the geometry and the bathymetry of the estuary are arbitrary and the parameters can be arbitrary functions of the horizontal coordinates, these equations have to be solved numerically. Here, we discuss the solution method used, the finite element method (FEM) approach, and the accuracy of the numerical solution.

To solve the equations using the FEM approach, the domain Ω is discretized using linear triangles. The discretized domain is denoted as $\Omega_{\tilde{h}}$, with $\tilde{h}$ the mean of the length of all the element edges in the discretized domain. The solution N is approximated as

$$N(x,y) \approx N_{\tilde{h}}(x,y) = \sum_{j=1}^{n} N_j \phi_j(x,y), \tag{27}$$

where $N_{\tilde{h}}$ is the finite element approximation of N. The total number of grid points (also called nodal points) is denoted by n, N_j are the amplitudes at nodal points j, and ϕ_j are the basis functions such that ϕ_j is zero at all nodal points except node j. Here, polynomials functions are chosen as basis functions. Inserting the approximation of N given by Eq. (27) in the weak formulation of the partial differential equation for the surface elevation gives a linear system of equations which can be solved for the unknown amplitudes N_j (see Kumar et al., 2016 for details).

In Kumar et al. (2016), three methods namely; DD-method, ZZ-method and mixed-method, were discussed to compute the first- and second-order partial derivatives of the surface elevation. It was shown that for the leading-order flow, the mixed-method which is a hybrid of DD-method and ZZ-method, works the best. However, partial derivatives of the leading-order flow are needed to compute the first-order water motion and the sediment availability, which is not possible with the mixed method. Therefore, we adopt the DD-method throughout the model to compute the partial derivatives of any order. Using the DD-method, the partial derivatives of N can be approximated by directly differentiating $N_{\tilde{h}}$ as

$$\frac{\partial^{a+b} N}{\partial x^a \partial y^b} \approx \frac{\partial^{a+b} N_{\tilde{h}}}{\partial x^a \partial y^b} = \sum_{j=1}^{n} N_j \frac{\partial^{a+b} \phi_j}{\partial x^a \partial y^b},$$

where a and b are the orders of differentiation in the x and y directions, respectively.

The accuracy of the finite element approximation $N_{\tilde{h}}$ and its partial derivatives depends on the degree of basis polynomials. In general, if polynomials of degree q are used, the numerical solution converges with rate $q+1$, the first-order partial derivatives with rate q and the second order partial derivatives with rate $q-1$ (see Gockenbach, 2006). Indeed, for the leading-order water motion, Kumar et al. (2016) has shown that using basis functions of order q_0, the surface elevation converges with rate q_0+1, the first-order partial derivatives with q_0 and second-order partial derivatives with rate q_0-1. Hence, the leading-order horizontal velocity (proportional to the first-order partial derivatives of the leading-order water motion) and vertical velocity (proportional to the second-order partial derivatives of the leading-order surface elevation) converge with rate q_0 and q_0-1, respectively.

In Sections 5–7, it was shown that to compute the first-order water motion and suspended sediment concentration, not only the leading-order flow components but their partial derivatives are required as these partial derivatives appear in the forcing terms for the first-order flow and first-order sediment concentration. For the

Table 5
The accuracy of the various components of the model when polynomials of degree q for the leading-order water motion and polynomials of degree at least $q-1$ for the first-order water motion and sediment availability, are used as basis functions.

Component		Accuracy
	η^0	$q+1$
$\boldsymbol{u}^0$	$\boldsymbol{u}_h^0$	q
	w^0	$q-1$
	η^1	$q-1$
	$\boldsymbol{u}_h^1$	$q-2$
	c^0	q
	c^1	$q-2$
	a	$q-2$

Table 6
Parameters for the years 1980 and 2005 for the Ems estuary (de Jonge et al., 2014).

Parameter	1980-value	2005-value
L	63.7 km	
L_b	30 km	
B_0	335 m	
H	10 m	
g	9.8 m s^{-2}	
f	1.34×10^{-4} s^{-1}	
ω	1.4×10^{-4} s^{-1}	
ρ_0	1020 kg m^{-3}	
ρ_s	2650 kg m^{-3}	
β	7.6×10^{-4} psu^{-1}	
A_{M_2}	1.43 m	1.35 m
A_{M_4}	0.25 m	0.19 m
ϕ	$-170.9°$	$-174.6°$
A_{v_0}	0.0184 m^2 s^{-1}	0.0135 m^2 s^{-1}
s_0	0.1421 m s^{-1}	0.0108 m s^{-1}
Q	80 m^3 s^{-1}	
w_s	1.0×10^{-3} m s^{-1}	
K_h	100 m^2 s^{-1}	
a_{total}	582 m^2	2710.8 m^2

first-order horizontal water motion to be q_1 accurate, the forcing terms must at least be q_1 accurate as well. Hence, it follows that q_0 must be at least equal to or larger than q_1+1, i.e., the degree of basis polynomials used to solve the leading-order water motion must be at least one higher than those used in the first-order water motion.

Table 5 lists the accuracy of different components of the model if polynomials of degree q are used as basis functions for the leading-order water motion and polynomials of degree $q-1$ are used as basis functions for the other components (i.e., first-order water surface elevation and sediment availability). If we take $q=3$, i.e., third degree polynomials as basis functions for the leading-order water motion and quadratic polynomials as basis functions for rest of the components, it follows from Table 5 that the sediment availability converges with rate 1.

10. Application to the Ems estuary

In this section, our new three-dimensional semi-idealized model is applied to investigate the spatial distribution of concentration and sediment availability in the Ems estuary under the condition of morphodynamic equilibrium. The Ems estuary is situated on the border of the Netherlands and Germany and has gone through various anthropogenic changes in the last few decades. Due to these interventions, the water motion and the sediment dynamics have changed significantly (de Jonge et al., 2014).

The Ems estuary is located between the island of Borkum in the North Sea and the weir at Herbrum and has a total length of approximately 100 km. In this paper, we only focus on the upper part of the Ems estuary, starting from Knock (Fig. 3). The length L of the estuary from Knock to Herbrum is approximately 63.7 km. Following Chernetsky et al. (2010), the geometry of the Ems estuary can be approximated as funnel-shaped with x and y denoting the along-channel and cross-channel coordinates, respectively. The along-channel coordinate varies from $x=0$ at the seaward side to $x=L$ at the river side. The lateral coordinate y varies between $y=-B(x)$ and $y=B(x)$, with $B(x)$ given by

$$B(x)=B_0e^{-x/L_b}.$$

Here, $2B_0$ is the total width at the seaward side and L_b is the e-folding length scale. The estuary is assumed to be well-mixed and the dynamic density ρ is assumed to vary as

$$\rho=\rho_0[1+\beta\ \tilde{s}(x)],$$

where $\tilde{s}(x)$ is the prescribed tidally- and depth-averaged salinity distribution obtained from Talke et al. (2009b) and $\beta=7.6\times10^{-4}$ psu^{-1} is a coefficient that relates salinity to density.

In this paper, two years (1980 and 2005) are studied. Following de Jonge et al. (2014), the bathymetric profiles for the years 1980 and 2005 are fitted with a fourth degree polynomial in the along-channel direction using observational data. Following Friedrichs and Hamrick (1996) and Schramkowski et al. (2002), the coefficient of vertical mixing A_v and the stress parameter s are parameterized as

$$(s,A_v)=(s_0,A_{v0})\frac{h}{H}.$$

Here A_{v0} and s_0 are the reference eddy viscosity and stress parameter, and H is the mean depth at the seaward side. The system is forced with a combination of M_2 and M_4 tides at the seaward side ($x=0$),

$$\eta=A_{M_2}\cos(\omega t)+A_{M_4}\cos(2\omega t-\phi),$$

where A_{M_2} and A_{M_4} are the elevation amplitudes defined in Section 3.2 and $\phi=\phi_{M_4}-2\phi_{M_2}$ is the relative phase between the M_2 and M_4 tidal constituents. In 1980, the mean tidal range at Knock was approximately 3.1 m with a relative phase of $-171.9°$. The tidal range in 2005 was 3.2 m with a relative phase of $-174.6°$ (see Chernetsky et al., 2010 for details). A constant river discharge of $Q=80$ m^3 s^{-1} is prescribed at the river boundary ($x=L$). A river discharge density Q' satisfying Eq. (11f) is defined as

$$Q'=\frac{Q}{2B|_{x=L}}.$$

Table 6 gives a list of all parameters used for the years 1980 and 2005 such that the observed M_2 water motion is well-reproduced by the model (see Kumar et al., 2016 for a discussion). Using these parameters, Table 7 lists the order of magnitude of various dimensionless parameters for the Ems estuary. Table 7 shows that the Ems estuary is tidally-dominated and river discharge gives a first-order contribution.

10.1. Laterally uniform bathymetry

The width-averaged bed profile of the Ems estuary for the years 1980 and 2005, used in de Jonge et al. (2014), are extended uniformly in the lateral direction (Fig. 4) to be used in the 3D semi-idealized model. The domain is discretized using approximately 100,000 nodes. A realistic value of the Coriolis parameter

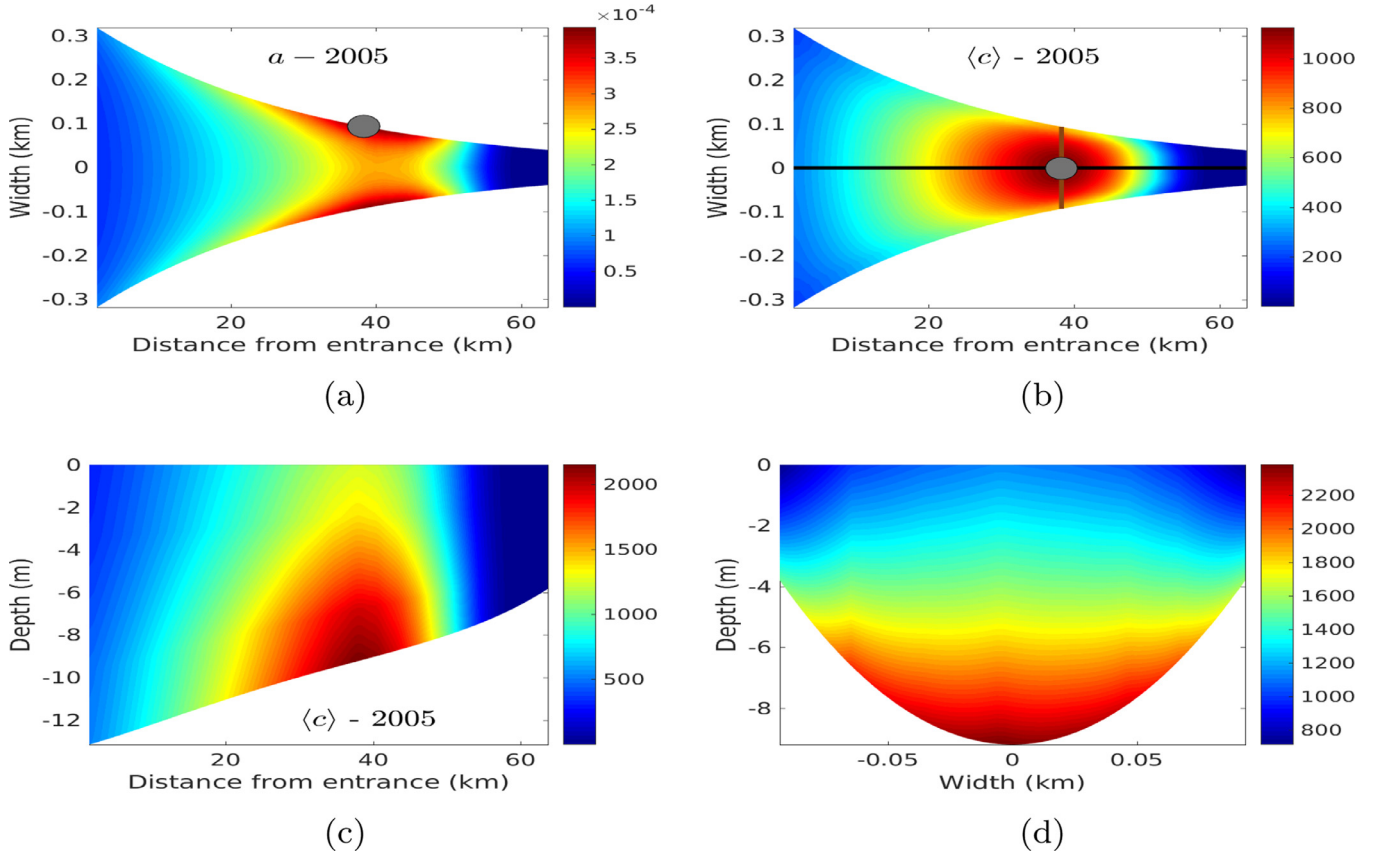

Fig. 8. Sediment availability and sediment concentration for 2005 with laterally varying bed profile. The *top left panel* shows the sediment availability (dimensionless) and *top right panel*, the sediment concentration (mg l^{-1}) at the surface. The black and chocolate lines pass through the location of maximum concentration at the surface in the x and y directions, respectively. The grey dot indicates the location of the maximum of the quantity being plotted. The *bottom left panel* shows the cross-sectional profile of the sediment concentration along the black line and the *bottom right panel*, along the chocolate line. (For interpretation of the references to colour in this figure legend, the reader is referred to the web version of this article.)

Table 7
Order of magnitude of dimensionless parameters for the Ems estuary.

Dimensionless parameter	1980	2005	Order
$\bar{A}_{M_2}/H = \epsilon$	0.14	0.13	$\mathcal{O}(\epsilon)$
$U/\omega L$	0.1		$\mathcal{O}(\epsilon)$
$\bar{A}_{M_4}/\bar{A}_{M_2}$	0.17	0.14	$\mathcal{O}(\epsilon)$
$gH/\omega^2 L^2$	1.22		$\mathcal{O}(1)$
U_d/U	0.1		$\mathcal{O}(\epsilon)$
$A_{v0}/\omega H^2$	1.31	0.96	$\mathcal{O}(1)$
$Q/\bar{Q}$	0.1		$\mathcal{O}(\epsilon)$
$w_s/\omega H$	0.71		$\mathcal{O}(1)$

$f = 1.34 \times 10^{-4}$ s^{-1}, corresponding to the Ems estuary, is used. The total amount of easily erodible sediment in the estuary a_{total} is chosen in such a way that the maximum concentration at the surface for 1980 and 2005 matches the observations, i.e., 400 mg l^{-1} for 1980 and 1000 mg l^{-1} for 2005 (from de Jonge et al. (2014)).

In Fig. 5, top panel, the distribution of easily erodible sediment in the Ems estuary is shown for the years 1980 and 2005.

Since the bed profile is laterally uniform, the sediment availability is also uniform in the lateral direction. The easily erodible sediment is concentrated close to the seaward side, approximately 6 km into the estuary, for the year 1980. For the year 2005, the easily erodible sediment is concentrated approximately 41 km away from the entrance and is more widely spread in the estuary than for 1980.

Next, we look at the tidally-averaged suspended sediment concentration at the surface. From Fig. 5, lower panel, it follows that for 1980, the maximum sediment concentration is found closer to the seaward side, approximately 7 km from the entrance and for 2005, at approximately 38 km from the entrance. The locations of maximum concentration are consistent with those found in Chernetsky et al. (2010), i.e., the ETM is found close to the seaward side for 1980 and more landward for 2005. Note that, because of the Coriolis parameter, the maximum availability of fine sediments and the maximum sediment concentration at the surface for both the years, shown by grey dots in Fig. 5, are found on the northern sides than in the middle of the channel.

10.2. Laterally varying bathymetry

In this experiment, the bathymetric profile in the lateral direction is varied parabolically requiring that the width-averaged depth remains the same as in the first experiment (Fig. 6). This preserves the mean depth of the channel in both the experiments. For both years, a_{total} used in the previous experiment is used.

From Figs. 7(a) and 8(a), it follows that the easily erodible sediments are not distributed uniformly in the lateral direction: the availability is much higher on the shallow sides than in the deeper channel for both years. However, the along-channel location of maximum availability is approximately the same as in the experiment with laterally uniform bathymetry. The maximum availability of fine sediments is higher for a laterally varying bed profile than for a laterally uniform bed profile.

For the year 1980, the maximum sediment concentration at the surface is found at approximately 8 km from the entrance (Fig. 7(b)) compared with 38 km for the year 2005 (Fig. 8(b)). The locations of maximum concentration move slightly landward for 1980 compared with the case with laterally uniform bed profile.

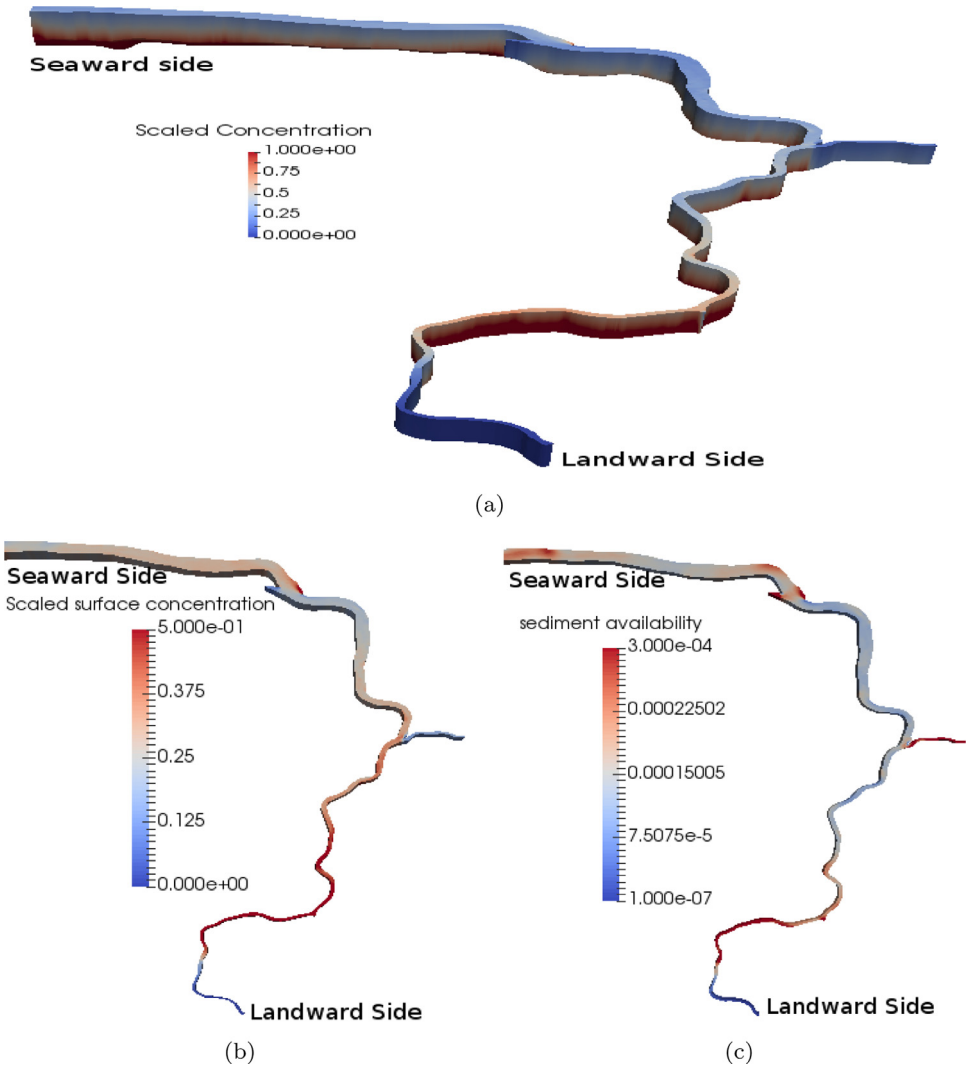

Fig. 9. The scaled three–dimensional suspended sediment concentration (a), surface concentration (b) and sediment availability (c) for the Ems estuary. (For interpretation of the references to colour in this figure legend, the reader is referred to the web version of this article.)

The maximum sediment concentrations are found in the middle of the channel even though the sediment availability is lower in the middle than on the shoals. Note that, unlike the case with laterally uniform bed profile, the Coriolis parameter does not significantly influence the location of the maximum concentration in the lateral direction. This is because the influence of laterally varying bathymetric profile on the longitudinal processes is stronger than those induced by the Coriolis force.

To illustrate the strength of the 3D model, the vertical profile of the sediment concentration is plotted in the along-channel and cross-channel directions passing through the location of maximum concentration at the surface. These locations are shown by black and chocolate lines in Fig. 7(b) for 1980 and Fig. 8(b) for 2005. The along-channel profile of the sediment concentration (Figs. 7(c) and 8(c)) shows that the region of high concentration is much wider at the bottom than at the surface. Moreover, the ETM in the along-channel direction is stronger and wider for 2005 than for 1980. The vertical profile of the sediment concentration in the cross-channel direction for 1980 and 2005 (Figs. 7(d) and 8(d)) depicts similar structure. Also, for both years, the maximum concentrations are found in the deepest parts of the channel, with maximum concentration at the bottom being almost two times the maximum concentration at the surface (Figs. 7(d) and 8(d)).

Using a realistic (but smoothed) bathymetry and geometry for the Ems estuary in 2005, the trapping of fine sediments is still mainly observed at the landward side of the estuary (see Fig. 9(a), and (b) in which only the (scaled) surface suspended sediment concentrations is shown), which qualitatively agrees with observations (de Jonge et al., 2014). In Fig. 9(c), the sediment availability in morphodynamic equilibrium is shown. Note that high sediment availability is not only found at locations where the suspended sediment concentrations are high, but also where tidal velocities are small (such as in the tributary).

11. Conclusions

A three-dimensional process-based semi-idealized model for estuarine turbidity maxima (ETM) in an estuary with arbitrary geometry and bathymetry has been developed. The water motion is driven by prescribed tidal forcing at the seaward side, and a river discharge at the river boundary. Furthermore, the horizontally varying, time- and depth-independent density field is prescribed (using, for example, observational data). The vertical eddy viscosity and diffusivity are assumed to be vertically constant and time-independent. Horizontal viscous effects are neglected. The resulting three-dimensional equations for water motion and suspended sediment concentration are scaled using typical scales, appropriate for the system under consideration. The physical variables are expanded in the small parameter ϵ which is the ratio of the mean amplitude of the M_2 surface elevation and the mean water depth

at the seaward boundary. This leads to a system of equations at each order of ϵ for the water motion and the suspended sediment concentration. Using rotating variables, the vertical profile of the velocity and the suspended sediment concentration can be obtained analytically in terms of the gradients of the surface elevation. To obtain the surface elevation at each order in ϵ, the continuity equation is integrated over the water column. This results in a two-dimensional elliptic partial differential equation for the surface elevation at that order. Using the concentrations and horizontal velocities, the horizontal sediment transport is calculated. The sediment still depends on the unknown sediment availability. By requiring the condition of morphodynamic equilibrium, an elliptic equation for the unknown sediment availability is obtained. These elliptic equations for the sediment availability and the surface elevation are solved numerically using the finite element method. In choosing the order of elements used for each order, special care is taken that the convergence rate of the numerical scheme used to calculate the sediment availability is at least of order one.

To test the model, we applied it to the Ems estuary with parameter values representative for years 1980 and 2005. The width is assumed to be exponentially convergent. The bathymetry in the longitudinal direction is taken from measurements and is approximated with a polynomial of degree four. In the first experiment, the bathymery is assumed to be uniform in the lateral direction. Focusing on the year 1980, the estuarine turbidity maximum (ETM) is found close to the seaward side. For the year 2005, the ETM is found far into the freshwater zone, approximately 38 km away from the entrance. This behaviour has been observed as well, indicating that the three-dimensional model is able to qualitatively reproduce the observed ETM behaviour in the Ems estuary. As a first indication of the importance of the lateral variations, the bed profile in the lateral direction is varied parabolically. For both 1980 and 2005 cases, the location of ETM remains approximately the same. However, the highest concentration is found in the middle of the channel even though most of the easily erodible sediment is found at the sides. This clearly demonstrates the importance of using a 3D model to compare the influence of lateral dynamics on the longitudinal processes. In this paper, we have mainly focused on the mathematical method used in the development of the model. In a forthcoming paper, the influence of bathymetric changes on each transport component will be discussed in detail, extending the sensitivity study of Schuttelaars et al. (2013) by including lateral depth variations. The idealized model developed in this paper is specifically aimed at studying estuaries in morphodynamic equilibrium, i.e., estuaries in which there are no convergences or divergences of sediment transport. To accommodate for the possibility of either a tidally-averaged import or export of sediment (due to, for example, the spring-neap cycle or human interventions), the condition of morphodynamic equilibrium has to be relaxed by allowing the sediment availability to vary on the long time scale, a model extension that is currently under investigation.

Acknowledgements

This work is part of the research programme NWO-ALW project 8843.10.005, which is financed by the Netherlands Organisation for Scientific Research (NWO) and the Chinese Organisation for Scientific Research (NSFC).

Appendix A. Scaling and perturbation analyses

A.1. Scaling analyses

To make the equations dimensionless, typical scales of the various quantities have to be introduced. The time t is made dimensionless using the frequency of the M_2 tidal constituent. In this paper, we focus on phenomena that vary on the estuarine length scale. Thus, as a length scale, the length L of the estuary is used. As a vertical length scale, the mean water depth H at the seaward side is used, defined as

$$H = \frac{1}{\mathrm{Len}(\partial_S\Omega)} \int_{\partial_S\Omega} h \, \mathrm{d}s, \tag{A.1}$$

where $\mathrm{Len}(\partial_S\Omega)$ denotes of the length of the seaward boundary. The local water depth h is also scaled with this parameter H. The typical scales for the surface elevation η, the vertical eddy viscosity A_v and the vertical diffusivity K_v by $\bar{A}$, $\bar{A}_\mathrm{v}$ and $\bar{K}_\mathrm{v}$, respectively, defined as

$$(\bar{A}, \bar{A}_\mathrm{v}, \bar{K}_\mathrm{v}) = \frac{1}{\mathrm{Len}(\partial_S\Omega)} \int_{\partial_S\Omega} (A_{M_2}, A_\mathrm{v}, K_\mathrm{v}) \, \mathrm{d}s. \tag{A.2}$$

The horizontal diffusivity K_h is assumed to be spatially uniform and constant in time.

The cross-sectionally averaged continuity equation is used to obtain a typical scale for the horizontal velocity $U = \frac{\bar{A}\omega L}{H}$. The typical scale W for the vertical velocity w follows from the assumption that all the terms in the three-dimensional continuity equation are of the same order of magnitude, i.e., $U/L = V/L = W/H$, implying that $W = HU/L$. Note that U is the dominant scale of the horizontal velocity in the tidally dominated estuaries. The typical magnitude for the density gradients ρ_x and ρ_y is denoted by ρ_H. The river discharge Q is made dimensionless by comparing it with the typical tidal discharge $\bar{Q}$, defined as

$$\bar{Q} = U \ \mathrm{Len}(\partial_R\Omega) \ H, \tag{A.3}$$

where $\mathrm{Len}(\partial_R\Omega)$ denotes the length of the river boundary.

Finally, the variables used for the concentration equation and the condition for morphodynamic equilibrium are scaled. First, the sediment availability is scaled by the mean amount of sediment available in the estuary for erosion:

$$\bar{a} = \frac{1}{\mathrm{Ar}(\Omega)} \iint_\Omega a \, \mathrm{d}\Omega, \tag{A.4}$$

where $\mathrm{Ar}(\Omega)$ denotes the total surface area of the estuary. Using this scale, and requiring that there is an approximate balance between erosion and deposition, it follows that a typical scale for the sediment concentration is given by

$$C = \frac{\rho_s s \bar{a} U}{g' d_s}. \tag{A.5}$$

The settling velocity w_s is scaled with $\bar{w}_\mathrm{s} = \omega H$, i.e., the dimensionless settling velocity w_s^* is the ratio of the tidal time scale and the deposition time scale. We define the parameter ϵ as the ratio of the mean elevation amplitude and the mean water depth at the seaward side, i.e.,

$$\epsilon = \bar{A}/H. \tag{A.6}$$

Using the dimensionless variables listed in Table A.8, the shallow water equations in the dimensionless form read,

$$\begin{aligned}
&u^*_{x^*} + v^*_{y^*} + w^*_{z^*} = 0,\\
&u^*_{t^*} + \epsilon(u^* u^*_{x^*} + v^* u^*_{y^*} + w^* u^*_{z^*}) - f^* v^*\\
&= -\left(\frac{L_g}{L}\right)^2 \eta^*_{x^*} - \frac{U_d}{U}(\epsilon\eta^* - z^*)\rho^*_x + \frac{1}{2}\mathrm{S}_\mathrm{v}^2 (A^*_\mathrm{v} u^*_{z^*})_{z^*},\\
&v^*_{t^*} + \epsilon(u^* v^*_{x^*} + v^* v^*_{y^*} + w^* v^*_{z^*}) + f^* u^*\\
&= -\left(\frac{L_g}{L}\right)^2 \eta^*_{y^*} - \frac{U_d}{U}(\epsilon\eta^* - z^*)\rho^*_y + \frac{1}{2}\mathrm{S}_\mathrm{v}^2 (A^*_\mathrm{v} v^*_{z^*})_{z^*}.
\end{aligned}$$

Here L_g is, apart from a factor 2π, the wavelength of the frictionless tidal wave, the vertical Stokes number $\mathrm{S}_\mathrm{v} = \sqrt{2\bar{A}_\mathrm{v}/\omega H^2}$ is the ratio of the frictional depth and the wavelength, and $U_d = \frac{gH\rho_H}{\rho_0\omega}$ is the scale for density driven residual circulation.

Table A.8
Non-dimensionalization of various physical quantities.

Physical quantity (Symbol)	Typical scale	Symbol	Dimensionless quantity
Domain			
Time (t)	M_2 frequency	ω	$t^* = \omega t$
Horizontal coordinates (x, y)	Estuarine length	L	$(x^*, y^*) = (x, y)/L$
Domain (Ω)	Estuarine length	L	$\Omega^* = \Omega/L$
Vertical coordinate (z)	Mean depth	H	$z^* = z/H$
Water depth (h)	Mean depth	H	$h^* = h/H$
Water motion			
Coriolis (f)	M_2 frequency	ω	$f^* = f/\omega$
Surface elevation (η)	Eq. (A.2)	$\bar{A}$	$\eta^* = \eta/\bar{A}$
Horizontal velocity (U, V)	Follows from cross-sectionally averaged continuity equation	$U = \frac{\bar{A}\omega L}{H}$	$(u^*, v^*) = (u, v)/U$
Vertical velocity (W)	Follows from three-dimensional continuity equation	$W = \frac{H}{L}U$	$w^* = w/W$
Eddy viscosity (A_v)	Eq. (A.2)	$\bar{A}_v$	$A_v^* = A_v/\bar{A}_v$
External forcing (A_{M_2}, A_{M_4})	Eq. (A.2)	$\bar{A}$	$(A_{M_2}^*, A_{M_4}^*) = (A_{M_2}, A_{M_4})/\bar{A}$
River discharge (Q)	Eq. (A.3)	$\bar{Q}$	$Q^* = Q/\bar{Q}$
Density gradients (ρ_x, ρ_y)	Typical magnitude	ρ_H	$(\rho_x^*, \rho_y^*) = (\rho_x, \rho_y)/\rho_H$
Sediment concentration			
Sediment availability (a)	Eq. (A.4)	$\bar{a}$	$a^* = a/\bar{a}$
Sediment concentration (c)	Eq. (A.5)	C	$c^* = c/C$
Vertical diffusivity (K_v)	Eq. (A.2)	$\bar{K}_v$	$K_v^* = K_v/\bar{K}_v$
Settling velocity (w_s)	Typical scale	$\bar{w}_s$	$w_s^* = w_s/\bar{w}_s$

The boundary condition at the seaward side (Eq. (2a)) becomes

$$\eta^* = A_{M_2}^* \cos(t^* - \phi_{M_2}) + A_{M_4}^* \cos(2t^* - \phi_{M_4}), \quad \text{for all } (x^*, y^*) \text{ in } \partial_S\Omega^*, \tag{A.7a}$$

where Ω^* denotes the domain in the dimensionless coordinates and $A_{M_2}^*$ and $A_{M_4}^*$ are defined in Table A.8. At the riverine boundary, we find

$$\int_{\partial_R\Omega} \left(\int_{-h^*}^{\epsilon\eta^*} \boldsymbol{u}_h^* \cdot \hat{\mathbf{n}} \, dz^* \right) ds^* = Q^*, \tag{A.7b}$$

where Q^* is defined in Eq. (A.4). At the lateral walls, we have

$$\int_{-h^*}^{\epsilon\eta^*} \boldsymbol{u}_h^* \cdot \hat{\mathbf{n}} \, dz^* = 0, \quad \text{for all } (x^*, y^*) \text{ in } \partial_L\Omega^*, \tag{A.7c}$$

At the free surface $z^* = \epsilon\eta^*$, the boundary conditions become,

$$w^* = \eta_{t^*}^* + \epsilon(u^*\eta_{x^*}^* + v^*\eta_{y^*}^*), \quad \text{and} \quad A_v^*(\boldsymbol{u}_h^*)_{z^*} = \mathbf{0}_h, \tag{A.7d}$$

and at the bottom $z^* = -h^*$, they read

$$w^* = -u^*h_{x^*}^* - v^*h_{y^*}^* \quad \text{and} \quad A_v^*(\boldsymbol{u}_h^*)_{z^*} = \frac{sH}{\bar{A}_v}\boldsymbol{u}_h^*. \tag{A.7e}$$

The three-dimensional advection-diffusion equation governing the suspended sediment concentration in dimensionless form reads,

$$c_{t^*}^* + \epsilon[(c^*u^*)_{x^*} + (c^*v^*)_{y^*} + (c^*w^*)_{z^*}] - \frac{K_h}{\omega L^2}\left[c_{x^*x^*}^* + c_{y^*y^*}^*\right] - \frac{\bar{K}_v}{\omega H^2}(K_v^* c_{z^*}^*)_{z^*} - w_s^* c_{z^*}^* = 0. \tag{A.8}$$

Since we assume that $K_v = A_v$, it follows that $\bar{K}_v/\omega H^2 = \frac{1}{2}S_v^2$. The boundary condition for suspended sediment concentration at the free surface reads

$$-\epsilon\frac{K_h}{\omega L^2}\left[c_{x^*}^*\eta_{x^*}^* + c_{y^*}^*\eta_{y^*}^*\right] + w_s^* c^* + \frac{\bar{K}_v}{\omega H^2}K_v^* c_{z^*}^* = 0, \quad \text{at } z^* = \epsilon\eta^*, \tag{A.9a}$$

and at the bottom

$$-\frac{K_h}{\omega L^2}(c_{x^*}^* h_{x^*}^* + c_{y^*}^* h_{y^*}^*) - \frac{\bar{K}_v}{\omega H^2}K_v^* c_{z^*}^* = w_s^* a^* \sqrt{u^{*2} + v^{*2}}, \quad \text{at } z^* = -h^*. \tag{A.9b}$$

Table A.9
Order of various dimensionless parameters appearing in the dimensionless equations for water motion, suspended sediment concentration and the condition of morphodynamic equilibrium. Refer to Table A.8 for definition of these parameters.

Dimensionless variables	Order
f^*	$\mathcal{O}(1)$
$U/\omega L = \epsilon$	$\mathcal{O}(\epsilon)$
L/L_g	$\mathcal{O}(1)$
U_d/U	$\mathcal{O}(\epsilon)$
$A_{M_2}^*$	$\mathcal{O}(1)$
$A_{M_4}^*$	$\mathcal{O}(\epsilon)$
Q^*	$\mathcal{O}(\epsilon)$
S_v	$\mathcal{O}(1)$
$sH/\bar{A}_v$	$\mathcal{O}(1)$
w_s^*	$\mathcal{O}(1)$
$K_h/\omega L^2$	$\mathcal{O}(\epsilon^2)$

The condition of morphodynamic equilibrium in the dimensionless form becomes,

$$\left\langle \frac{\partial}{\partial x^*}\int_{-h^*}^{\epsilon\eta^*}\left(\epsilon c^*u^* - \frac{K_h}{\omega L^2}c_{x^*}^*\right)dz^* + \frac{\partial}{\partial y^*}\int_{-h^*}^{\epsilon\eta^*}\left(\epsilon c^*v^* - \frac{K_h}{\omega L^2}c_{y^*}^*\right)dz^* \right\rangle = 0. \tag{A.10}$$

A.2. Perturbation analyses

For the estuaries under consideration, the typical elevation amplitude is much smaller than the typical water depth,

$$\epsilon = \frac{\bar{A}}{H} \ll 1. \tag{A.11}$$

Using this information, we can asymptotically expand the vector of unknown physical variables $\boldsymbol{\psi}^* = (\eta^*, u^*, v^*, w^*, c^*)$ as

$$\boldsymbol{\psi}^* = \boldsymbol{\psi}^{0*} + \epsilon\boldsymbol{\psi}^{1*} + \epsilon^2\boldsymbol{\psi}^{2*} + \ldots. \tag{A.12}$$

Next, the asymptotic expansion is substituted in the scaled equations and the dimensionless coefficients appearing in these scaled equations are related to different orders in ϵ. A full list of these dimensionless coefficients is given in Table A.9. In the following, we

are going to derive the differential problems for the water motion and suspended sediment concentration, at subsequent orders in ϵ.

With the assumption that $\epsilon \ll 1$, the boundary conditions and integrals evaluated at $z^* = \epsilon\eta^*$ can be simplified. For boundary conditions at river boundary and lateral walls, the integrals from $z^* = -h^*$ to $z^* = \epsilon\eta^*$ can be split into two integrals with limits ranging from $z^* = -h^*$ to $z^* = 0$ and from $z^* = 0$ to $z^* = \epsilon\eta^*$. By using the Taylor expansion of u^* and v^* around $z^* = 0$ in the latter integral, the boundary conditions at the river side and lateral boundaries reduce to

$$\int_{\partial_R\Omega^*}\left[\int_{-h^*}^{0}\boldsymbol{u}_{\mathrm{h}}^*\cdot\hat{\mathbf{n}}\,\mathrm{d}z^* + \epsilon\eta^*\boldsymbol{u}_{\mathrm{h}}^*|_{z^*=0}\cdot\hat{\mathbf{n}}\right]\mathrm{d}s^* + \mathcal{O}(\epsilon^2) = -Q^*. \tag{A.13}$$

$$\int_{-h^*}^{0}\boldsymbol{u}_{\mathrm{h}}^*\cdot\hat{\mathbf{n}}\,\mathrm{d}z^* + \epsilon\eta^*\boldsymbol{u}_{\mathrm{h}}^*|_{z^*=0}\cdot\hat{\mathbf{n}} + \mathcal{O}(\epsilon^2) = 0, \quad \text{for all } (x^*, y^*) \text{ in } \partial_C\Omega^*, \tag{A.14}$$

where $\mathcal{O}(\epsilon^2)$ denotes all the terms of the order two or more. Using the same approach, the dimensionless dynamic and kinematic boundary conditions at the free surface $z^* = \epsilon\eta^*$ can be rewritten as

$$w^* + \epsilon\eta^* w_{z^*}^* + \mathcal{O}(\epsilon^2) = \eta_{t^*}^* + \epsilon(u^*\eta_{x}^* + v^*\eta_{y}^*) + \mathcal{O}(\epsilon^2), \quad \text{at } z^* = 0, \tag{A.15}$$

$$A_{\mathrm{v}}^*(\boldsymbol{u}_{\mathrm{h}}^*)_{z^*} + \epsilon A_{\mathrm{v}}^*\eta^*(\boldsymbol{u}_{\mathrm{h}}^*)_{z^*z^*} + \mathcal{O}(\epsilon^2) = \mathbf{0}_{\mathrm{h}}, \quad \text{at } z^* = 0. \tag{A.16}$$

The boundary condition for the suspended sediment concentration at the free surface becomes,

$$\begin{aligned}
&-\epsilon\frac{K_{\mathrm{h}}}{\omega L^2}[c^* + \epsilon\eta^* c_{z^*}^* + \mathcal{O}(\epsilon^2)]_{x^*}\eta_{x^*}^* \\
&-\epsilon\frac{K_{\mathrm{h}}}{\omega L^2}[c^* + \epsilon\eta^* c_{z^*}^* + \mathcal{O}(\epsilon^2)]_{y^*}\eta_{y^*}^* \\
&+w_s^*[c^* + \epsilon\eta^* c_{z^*}^* + \mathcal{O}(\epsilon^2)] + \frac{\bar{K}_{\mathrm{v}}}{\omega H^2}K_{\mathrm{v}}^*[c_{z^*}^* \\
&+\epsilon\eta^* c_{z^*z^*}^* + \mathcal{O}(\epsilon^2)], \quad \text{at } z^* = 0.
\end{aligned} \tag{A.17}$$

Next, the asymptotic expansion of unknown physical variables given by Eq. (A.12) is substituted into the governing equations for water motion, suspended sediment concentration and the condition of morphodynamic equilibrium. Using Table A.9, dimensionless systems of equations are found at different orders of ϵ by collecting terms of equal order.

Leading-order water motion. The leading-order (ϵ^0) system of equations for water motion in the dimensionless form is given by

$$\begin{aligned}
&u_{x^*}^{0*} + v_{y^*}^{0*} + w_{z^*}^{0*} = 0, \\
&u_{t^*}^{0*} - f^*v^{0*} = -\left(\frac{L_g}{L}\right)^2\eta_{x^*}^{0*} + \frac{1}{2}\mathrm{S}_{\mathrm{v}}^2(\bar{A}_{\mathrm{v}}u_{z^*}^{0*})_{z^*}, \\
&v_{t^*}^{0*} + f^*u^{0*} = -\left(\frac{L_g}{L}\right)^2\eta_{y^*}^{0*} + \frac{1}{2}\mathrm{S}_{\mathrm{v}}^2(\bar{A}_{\mathrm{v}}v_{z^*}^{0*})_{z^*},
\end{aligned}$$

together with boundary conditions

$$\begin{aligned}
&A_{\mathrm{v}}^*(\boldsymbol{u}_{\mathrm{h}}^{0*})_{z^*} = \mathbf{0}_{\mathrm{h}}, \quad \text{and } w^{0*} = \eta_t^{0*}, \quad \text{at } z^* = 0, \\
&A_{\mathrm{v}}^*(\boldsymbol{u}_{\mathrm{h}}^{0*})_{z^*} = \tfrac{Hs}{\bar{A}_{\mathrm{v}}}\boldsymbol{u}_{\mathrm{h}}^{0*}, \quad \text{and } w^{0*} = -u^{0*}h_{x^*}^* - v^{0*}h_{y^*}^*, \quad \text{at } z^* = -h^*, \\
&\eta^{0*} = A_{M_2}^*\cos(t^*) \quad \text{for all } (x^*, y^*) \text{ in } \partial_S\Omega^*, \\
&\textstyle\int_{\partial_R\Omega^*}\left(\int_{-h^*}^{0}\boldsymbol{u}_{\mathrm{h}}^{0*}\cdot\hat{\mathbf{n}}\,\mathrm{d}z^*\right)\mathrm{d}s^* = 0, \\
&\textstyle\int_{-h^*}^{0}\boldsymbol{u}_{\mathrm{h}}^{0*}\cdot\hat{\mathbf{n}}\,\mathrm{d}z^* = 0, \quad \text{for all } (x^*, y^*) \text{ in } \partial_C\Omega^*.
\end{aligned}$$

First-order water motion. The first-order (ϵ^1) system of equations for the water motion is given by

$$\begin{aligned}
&u_{x^*}^{1*} + v_{y^*}^{1*} + w_{z^*}^{1*} = 0, \\
&u_{t^*}^{1*} + u^{0*}u_{x^*}^{0*} + v^{0*}u_{y^*}^{0*} + w^{0*}u_{z^*}^{0*} - f^*v^{1*} \\
&= -\left(\frac{L_g}{L}\right)^2\eta_{x^*}^{1*} + \frac{U_d}{U}z^*\rho_x^* \\
&+\frac{1}{2}\mathrm{S}_{\mathrm{v}}^2(\bar{A}_{\mathrm{v}}u_{z^*}^{1*})_{z^*}, \\
&v_{t^*}^{1*} + u^{0*}v_{x^*}^{0*} + v^{0*}v_{y^*}^{0*} + w^{0*}v_{z^*}^{0*} + f^*u^{1*} \\
&= -\left(\frac{L_g}{L}\right)^2\eta_{y^*}^{1*} + \frac{U_d}{U}z^*\rho_y^* \\
&+\frac{1}{2}\mathrm{S}_{\mathrm{v}}^2(\bar{A}_{\mathrm{v}}u_{z^*}^{1*})_{z^*},
\end{aligned}$$

with boundary conditions

$$\begin{aligned}
&(\boldsymbol{u}_{\mathrm{h}}^{1*})_{z^*} = -\eta^{0*}(\boldsymbol{u}_{\mathrm{h}}^{0*})_{z^*z^*}, \\
&w^{1*} = \eta_t^{1*} - (\eta^{0*}w_{z^*}^{0*} - u^{0*}\eta_{x^*}^{0*} - v^{0*}\eta_{y^*}^{0*}) \ \text{ at } z^* = 0, \\
&A_{\mathrm{v}}^*(\boldsymbol{u}_{\mathrm{h}}^{1*})_{z^*} = \frac{Hs}{\bar{A}_{\mathrm{v}}}\boldsymbol{u}_{\mathrm{h}}^{1*}, \\
&\text{and } w^{1*} = -u^{1*}h_{x^*}^* - v^{1*}h_{y^*}^* \ \text{ at } z^* = -h^*, \\
&\eta^{1*} = A_{M_4}^*\cos(2t^* - \phi) \ \text{ for all } (x^*, y^*) \text{ in } \partial_S\Omega^*, \\
&\int_{\partial_R\Omega^*}\left[\int_{-h^*}^{0}\boldsymbol{u}_{\mathrm{h}}^{1*}\cdot\hat{\mathbf{n}}\,\mathrm{d}z^* + \eta^{0*}\boldsymbol{u}_{\mathrm{h}}^{0*}|_{z^*=0}\cdot\hat{\mathbf{n}}\right]\mathrm{d}s^* = -Q^*, \\
&\int_{-h^*}^{0}\boldsymbol{u}_{\mathrm{h}}^{1*}\cdot\hat{\mathbf{n}}\,\mathrm{d}z^* + \eta_0^*\boldsymbol{u}_{\mathrm{h}}^{0*}|_{z^*=0}\cdot\hat{\mathbf{n}} = 0, \quad \text{for all } (x^*, y^*) \text{ in } \partial_C\Omega^*.
\end{aligned}$$

Leading-order suspended sediment concentration. The leading-order (ϵ^0) system of equations for the suspended sediment concentration is given by

$$c_{t^*}^{0*} - \frac{\bar{K}_{\mathrm{v}}}{\omega H^2}\left(K_{\mathrm{v}}^*c_{z^*}^{0*}\right)_{z^*} - (w_s^*c^{0*})_{z^*} = 0,$$

with boundary conditions

$$\begin{aligned}
&-\frac{\bar{K}_{\mathrm{v}}}{\omega H^2}K_{\mathrm{v}}^*c_{z^*}^{0*} = w_s^*c^{0*}, \quad \text{at } z^* = 0, \\
&-\frac{\bar{K}_{\mathrm{v}}}{\omega H^2}K_{\mathrm{v}}^*c_{z^*}^{0*} = w_s^*a^*|\boldsymbol{u}_{\mathrm{h}}^{0*}|, \quad \text{at } z^* = -h^*.
\end{aligned}$$

The above equation shows that the leading-order suspended sediment concentration is solely governed by the absolute value of the leading-order horizontal velocity.

First-order suspended sediment concentration. The first-order (ϵ^1) system of equations for the suspended sediment concentration is given by

$$c_{t^*}^{1*} + u^{0*}c_{x^*}^{0*} + v^{0*}c_{y^*}^{0*} + w^{0*}c^{0*}z^* - \frac{\bar{K}_{\mathrm{v}}}{\omega H^2}\left(K_{\mathrm{v}}^*c_{z^*}^{1*}\right)_{z^*} - (w_s^*c^{1*})_{z^*} = 0,$$

with boundary conditions

$$\begin{aligned}
&\frac{\bar{K}_{\mathrm{v}}}{\omega H^2}K_{\mathrm{v}}^*\left[c_{z^*}^{1*} + \eta_0^*c_{z^*z^*}^{0*}\right] + w_s^*\left[c^{1*} + \eta^{0*}c_{z^*}^{0*}\right] = 0 \ \text{ at } z = 0, \\
&\frac{\bar{K}_{\mathrm{v}}}{\omega H^2}K_{\mathrm{v}}^*c_{z^*}^{1*} + w_s^*a^*\frac{\boldsymbol{u}_{\mathrm{h}}^{0*}\cdot\boldsymbol{u}_{\mathrm{h}}^{1*}}{|\boldsymbol{u}_{\mathrm{h}}^{0*}|} = 0, \quad \text{at } z^* = -h^*.
\end{aligned}$$

Note that the boundary condition at the bottom $z^* = -h^*$ contains the first-order horizontal velocity $\boldsymbol{u}_{\mathrm{h}}^{1*}$, which as we have seen in the main text (Eq. (19)), can be written as a sum of various components. It means that the first-order suspended sediment concentration due to the bed shear stress can also be written as sum of various components, one corresponding to each component of the first-order horizontal velocity.

Appendix B. Suspended sediment concentration

Leading-order suspended sediment concentration. The equation governing the leading-order suspended sediment concentration is given by

$$c_t^{0n} - (w_s c^{0n})_z - (K_v c_z^{0n})_z = 0, \quad n = 4m, \text{ where, } m = 0, 1, 2, \ldots$$

such that,

$$K_v c_z^{0n} + w_s c^{0n} = 0 \quad \text{at} \quad z = 0,$$

$$K_v c_z^{0n} + a\frac{w_s \rho_s}{\rho_0 g' d_s} \Re\{\tilde{\boldsymbol{\tau}}_b{}^{0n} e^{\frac{ni\omega t}{2}}\} = 0 \quad \text{at} \quad z = -h,$$

where $\Re\{\tilde{\boldsymbol{\tau}}_b{}^{0n} e^{\frac{ni\omega t}{2}}\}$ is the nth order harmonics of the absolute value of the leading-order bed shear stress $|\boldsymbol{\tau}_b|^0$. Assuming $c^{0n} = \Re\{C^{0n} e^{\frac{ni\omega t}{2}}\}$, the above equation becomes

$$(K_v C_z^{0n})_z + w_s C_z^{0n} - \frac{ni\omega}{2} C^{0n} = 0.$$

Since $K_v := K_v(x, y)$ and K_h is constant, and using that the above equation is a linear second-order ordinary differential equation in the vertical coordinate z, it can be solved analytically in the vertical for C^{0n}:

$$C^{0n}(x, y, z) = A^{0n}(x, y) e^{r_{n,1} z} + B^{0n}(x, y) e^{r_{n,2} z},$$

where $r_{n,1}$ and $r_{n,2}$ are the roots of the quadratic polynomial equation: $K_v r_n^2 + w_s r_n - \frac{ni\omega}{2} = 0$, and $A^{0n}(x,y)$ and $B^{0n}(x,y)$ are given by

$$A^{0n} = -B^{0n}\frac{w_s + K_v r_{n,2}}{w_s + K_v r_{n,1}},$$

$$B^{0n} = a\frac{w_s \rho_s \tilde{\boldsymbol{\tau}}_b{}^{0n}}{\rho_0 g' d_s K_v}\left[\frac{w_s + K_v r_{n,1}}{r_{n,1} e^{-r_{n,1}h}(w_s + K_v r_{n,2}) - r_{n,2} e^{-r_{n,2}h}(w_s + K_v r_{n,1})}\right].$$

We can rewrite c^0 as

$$c^0 = a\tilde{c}^0,$$

where $\tilde{c}^0$ is the solution of the leading-order suspended sediment concentration with $a = 1$.

First-order suspended sediment concentration. The equation governing the first-order suspended sediment concentration c^1 is given by

$$c_t^1 + F_{AC}^c - (K_v c_z^1)_z - (w_s c^1)_z = 0, \tag{B.1a}$$

where $F_{AC}^c = u^0 c_x^0 + v^0 c_y^0 + w^0 c_z^0$. At the surface, the boundary condition reads

$$w_s c^1 + K_v c_z^1 = F_S^c, \quad \text{at } z = 0, \tag{B.1b}$$

where $F_S^c = -\eta_0\left[w_s c_z^0 + K_v c_{zz}^0\right]$. At the bottom, the boundary condition reads

$$K_v c_z^1 + a\frac{w_s \rho_s}{\rho_0 g' d_s}|\boldsymbol{\tau}_b|^1 = 0, \quad \text{at } z = -h. \tag{B.1c}$$

Here $|\boldsymbol{\tau}_b|^1$ denotes the first-order component of the absolute value of the bed shear stress. Next, the first-order suspended sediment concentration is solved each forcing term individually.

Contribution due to advection. The forcing term F_{AC}^c appearing in Eq. (B.1) is generated by the interaction of leading-order velocity and the leading-order suspended sediment concentration can be expressed as

$$F_{AC}^c = aF_{AC}^a + a_x F_{AC}^{a_x} + a_y F_{AC}^{a_y},$$

where $F_{AC}^a = \tilde{c}_x^{0a} u^0 + \tilde{c}_y^{0a} v^0 + \tilde{c}_z^{0a} w^0$, $F_{AC}^{a_x} = \tilde{c}^{0a} u^0$, and $F_{AC}^{a_y} = \tilde{c}^{0a} v^0$ are the components proportional to a, a_x, and a_y, respectively. Since we are interested in the M_2 constituent of the first-order concentration, we can write

$$(F_{AC}^a, F_{AC}^{a_x}, F_{AC}^{a_y}, c_{AC}^{12}) = \Re\{(f_{AC}^a, f_{AC}^{a_x}, f_{AC}^{a_y}, C_{AC}^{12}) e^{i\omega t}\}.$$

Now, the governing equation becomes,

$$(K_v C_{AC,z}^{12})_z + w_s C_{AC,z}^{12} - i\omega C_{AC}^{12} = af^c + a_x f_{AC}^{a_x} + a_y f_{AC}^{a_y}, \tag{B.2}$$

with boundary conditions

$$K_v c_{AC,z}^{12} + w_s C_{AC}^{12} = 0, \quad \text{at } z = 0,$$
$$K_v c_{AC,z}^{12} = 0 \quad \text{at } z = -h.$$

This equation can be solved analytically for C_{AC}^{12} for each forcing $\tilde{f}$ on the right hand side separately using the method of variation of parameters, resulting in

$$C_{AC}^{12}(x, y, z) = Ae^{r_1 z} + Be^{r_2 z} + \frac{1}{r_2 - r_1}\int_{-h}^{z}[e^{r_2(z-z')} - e^{r_1(z-z')}]\tilde{f}(z')\, \mathrm{d}z',$$

where r_1, r_2 are the roots of the quadratic polynomial

$$K_v r^2 + w_s r - i\omega = 0,$$

and coefficients A and B are given as

$$A = -\frac{r_2 e^{-r_2 h}}{r_2 - r_1}\int_{-h}^{0}\left[\frac{(K_v r_2 + w_s)e^{-r_2 z} - (K_v r_1 + w_s)e^{-r_1 z}}{r_2(K_v r_1 + w_s)e^{-r_2 h} - r_1(K_v r_2 + w_s)e^{-r_1 h}}\right]\tilde{f}(z)\, \mathrm{d}z,$$

$$B = -A\frac{r_1}{r_2}e^{(r_2 - r_1)h}.$$

The complete solution can be written as

$$C_{AC}^{12} = a\tilde{C}_{AC}^{12,a} + a_x\tilde{C}_{AC}^{12,a_x} + a_y\tilde{C}_{AC}^{12,a_y},$$

where $\tilde{C}_{AC}^{12,a}$, $\tilde{C}_{AC}^{12,a_x}$ and $\tilde{C}_{AC}^{12,a_y}$ are the solutions of the above equation for $a = 1$, $a_x = 1$ and $a_y = 1$, respectively. Note that when computing the solution for $a = 1$, a_x and a_y are set to zero. The similar strategy holds when computing the solution for $a_x = 1$ ($a = 0$ and $a_y = 0$) and $a_y = 1$ ($a = 0$ and $a_x = 0$). The M_2 concentration c_{AC}^{12} can thus be expressed as

$$c_{AC}^{12} = a\tilde{c}_{AC}^{12,a} + a_x\tilde{c}_{AC}^{12,a_x} + a_y\tilde{c}_{AC}^{12,a_y},$$

where,

$$(\tilde{c}_{AC}^{12,a}, \tilde{c}_{AC}^{12,a_x}, \tilde{c}_{AC}^{12,a_y}) = \Re\{(\tilde{C}_{AC}^{12,a}, \tilde{C}_{AC}^{12,a_x}, \tilde{C}_{AC}^{12,a_y}) e^{i\omega t}\}.$$

Contribution due to first-order bed-shear stress. See the main text.

Contribution due to forcing at the surface. The M_2 component of the surface boundary contribution $F_S^c = -\eta^0\left[w_s c_z^0 + K_v c_{zz}^0\right]$ can be expressed at $\Re\{af_S^c e^{i\omega t}\}$. Writing $c_S^{12} = \Re\{C_S^{12} e^{i\omega t}\}$, the equation governing the first-order sediment concentration due to forcing at the surface reads

$$(w_s C_S^{12})_z + (K_v C_{S,z}^{12})_z - i\omega C_S^{12} = 0,$$

together with the boundary conditions,

$$K_v C_{S,z}^{12} + w_s C_S^{12} = af_S^c, \quad \text{at } z = 0,$$
$$K_v C_{S,z}^{12} = 0, \quad \text{at } z = -h.$$

This equation can be solved analytically in the vertical as

$$C_S^{12} = Ae^{r_1 z} + Be^{r_2 z},$$

where r_1, r_2 are the roots of the polynomial $K_v r^2 + w_s r - i\omega = 0$ and the coefficients A and B are given by

$$A = a\left[\frac{r_2 r^{r_1 h}}{r_2(w_s + K_v r_1)e^{r_1 h} - r_1(w_s + K_v r_2)e^{r_2 h}}\right]f_S^c,$$

$$B = -A\frac{r_1}{r_2}e^{(r_2 - r_1)h}.$$

Appendix C. Condition of morphodynamic equilibrium

The condition of morphodynamic equilibrium reads

$$\left\langle \frac{\partial}{\partial x}\int_{-h}^{\eta}\left(cu - K_h\frac{\partial c}{\partial x}\right)\mathrm{d}z + \frac{\partial}{\partial y}\int_{-h}^{\eta}\left(cv - K_h\frac{\partial c}{\partial y}\right)\mathrm{d}z\right\rangle = 0. \quad \text{(C.1)}$$

Using the dimensionless variables introduced in Eq. (A.8) of Appendix A, the above equation becomes

$$\left\langle \frac{\partial}{\partial x^*}\int_{-h^*}^{\epsilon\eta^*}\left(\epsilon c^*u^* - \frac{K_h}{\omega L^2}c^*_{x^*}\right)\mathrm{d}z^* + \frac{\partial}{\partial y^*}\int_{-h^*}^{\epsilon\eta^*}\left(\epsilon c^*v^* - \frac{K_h}{\omega L^2}c^*_{y^*}\right)\mathrm{d}z^*\right\rangle = 0. \quad \text{(C.2)}$$

First, we will consider the first term in Eq. (C.2). The integral from $z^* = -h^*$ to $z^* = \epsilon\eta^*$ can be split into two integrals; one from $z^* = -h^*$ to $z^* = 0$ and one from $z^* = 0$ to $z^* = \epsilon\eta^*$ as,

$$\int_{-h^*}^{\epsilon\eta^*} c^*u^*\ \mathrm{d}z^* = \int_{-h^*}^{0} c^*u^*\ \mathrm{d}z^* + \int_{0}^{\epsilon\eta^*} c^*u^*\ \mathrm{d}z^*.$$

The asymptotic expansions of c^* and u^* can be used directly in the first integral,

$$\int_{-h^*}^{0} c^*u^*\ \mathrm{d}z^* = \int_{-h^*}^{0}\left[c^{0*}u^{0*} + \epsilon(c^{0*}u^{1*} + c^{1*}u^{0*}) + \mathcal{O}(\epsilon^2)\right]\mathrm{d}z^*,$$

while for the second integral, c^* and u^* are first expanded around $z^* = 0$ using the Taylor series expansion and then asymptotic expansions of c^* and u^* are used,

$$\begin{aligned}\int_{0}^{\epsilon\eta^*} c^*u^*\ \mathrm{d}z^* &= \int_{0}^{\epsilon\eta^*}[(c^*u^*)|_{z^*=0} + z^*(c^*u^*)_{z^*}|_{z^*=0} + \ldots]\mathrm{d}z^*,\\ &= \epsilon\left[\eta^*(c^*u^*)|_{z^*=0} + \epsilon\frac{\eta^{*2}}{2}(c^*u^*)_{z^*}|_{z^*=0} + \mathcal{O}(\epsilon^2)\right],\\ &= \epsilon\eta^{0*}c^{0*}u^{0*}|_{z^*=0} + \epsilon^2\left[\eta^{0*}c^{0*}u^{1*}|_{z^*=0} + \eta^{0*}c^{1*}u^{0*}|_{z^*=0}\right.\\ &\quad \left. + \eta^{1*}c^{0*}u^{0*}|_{z^*=0} + \frac{(\eta^{0*})^2}{2}(c^{0*}u^{0*})_{z^*}|_{z^*=0}\right] + \mathcal{O}(\epsilon^3).\end{aligned}$$

Hence, we have

$$\left\langle \int_{-h^*}^{\epsilon\eta^*} c^*u^*\ \mathrm{d}z^*\right\rangle = \int_{-h^*}^{0}\langle c^{0*}u^{0*}\rangle\mathrm{d}z^* + \epsilon\left[\int_{-h^*}^{0}\langle c^{0*}u^{1*} + c^{1*}u^{0*}\rangle\ \mathrm{d}z^* + \langle\eta^{0*}c^{0*}u^{0*}|_{z^*=0}\rangle\right] + \mathcal{O}(\epsilon^2).$$

Since the leading order concentration itself consists of M_0 and M_4 contributions i.e., $c^{0*} = c^{00*} + c^{04*}$, and the leading-order water motion is semi-diurnal (M_2), the leading-order contribution is $c^{0*}u^{0*} = c^{00*}u^{02*} + c^{04*}u^{02*}$. The first term $c^{00*}u^{02*}$ gives an M_2 signal and the second term $c^{04*}u^{02*}$ both an M_2 and M_6 signal. When averaged over the tidal period, these contributions vanish i.e., $< c^{00*}u^{02*} > = < c^{04*}u^{02*} > = 0$, implying that $\langle c^{0*}u^{0*}\rangle = 0$.

The first-order velocity u^{1*} consists of an M_0 and M_4 contributions, resulting in

$$\begin{aligned}c^{0*}u^{1*} &= (c^{00*} + c^{04*})(u^{10*} + u^{14*})\\ &= c^{00*}u^{10*} + c^{00*}u^{14*} + c^{04*}u^{10*} + c^{04*}u^{14*}.\end{aligned}$$

In the above expression, on the extreme right, the first term gives an M_0 contribution, the second and third terms both give M_4 contributions, and the fourth term gives an M_0 and M_4 contribution. When averaged over a tidal period, all contributions vanish except the residual (M_0) ones, i.e., $\langle c^{0*}u^{1*}\rangle = c^{00*}u^{10*} + \langle c^{04*}u^{14*}\rangle$.

The first-order suspended sediment concentration contains an M_2 contribution i.e.,$c^{1*} = c^{12*}$, resulting in $\langle c^{1*}u^{0*}\rangle = \langle c^{12*}u^{02*}\rangle$. Using this information, it follows that

$$\begin{aligned}&\left\langle \int_{-h^*}^{\epsilon\eta^*} c^*u^*\ \mathrm{d}z^*\right\rangle\\ &= \epsilon\left[\int_{-h^*}^{0} c^{00*}u^{10*} + \langle c^{04*}u^{14*} + c^{12*}u^{02*}\rangle\ \mathrm{d}z^*\right.\\ &\quad \left. + \langle\eta^{0*}c^{0*}u^{0*}|_{z^*=0}\rangle\right] + \mathcal{O}(\epsilon^2)\end{aligned}$$

.

Next, we will derive the leading-order contribution to the second term in Eq. (C.2). Again, we split the integral in two parts:

$$\int_{-h^*}^{\epsilon\eta^*} c^*_{x^*}\mathrm{d}z^* = \int_{-h^*}^{0} c^*_{x^*}\mathrm{d}z^* + \int_{0}^{\epsilon\eta^*} c^*_{x^*}\mathrm{d}z^*.$$

Using the same approach as above, we find that

$$\left\langle \int_{-h^*}^{\epsilon\eta^*} c^*_{x^*}\mathrm{d}z^*\right\rangle = \int_{-h^*}^{0}\langle c^{0*}_{x^*}\rangle\mathrm{d}z^* + \epsilon\left[\int_{-h^*}^{0}\langle c^{1*}_{x^*}\rangle\mathrm{d}z^* + \langle\eta^{0*}(c^{0*}|_{z^*=0})_{x^*}\rangle\right] + \mathcal{O}(\epsilon^2).$$

In a similar way as above, we find that

$$\begin{aligned}c^{0*} &= c^{00*} + c^{04*} \Rightarrow \langle c^{0*}_{x^*}\rangle = c^{00*}_{x^*},\\ c^{1*} &= c^{12*} \Rightarrow \langle c^{1*}_{x^*}\rangle = 0,\\ \eta^{0*}c^{0*} &= \eta^{02*}(c^{00*} + c^{04*}) = \underbrace{\eta^{02*}c^{00*}}_{M_2} + \underbrace{\eta^{02*}c^{04*}}_{M_2+M_6} \Rightarrow \langle\eta^{0*}c^{0*}\rangle = 0.\end{aligned}$$

Hence the second term in Eq. (C.2) after averaging over a tidal period becomes,

$$\left\langle \int_{-h^*}^{\epsilon\eta^*} c^*_{x^*}\mathrm{d}z^*\right\rangle = \int_{-h^*}^{0} c^{00*}_{x^*}\mathrm{d}z^* + \mathcal{O}(\epsilon^2).$$

Hence we obtain,

$$\begin{aligned}&\left\langle \partial_{x^*}\int_{-h^*}^{\epsilon\eta^*}\left(\epsilon c^*u^* - \frac{K_h}{\omega L^2}c^*_{x^*}\right)\mathrm{d}z^*\right\rangle\\ &= \epsilon^2\partial_{x^*}\left[\int_{-h^*}^{0} c^{00*}u^{10*} + \langle c^{04*}u^{14*} + c^{12*}u^{02*}\rangle\ \mathrm{d}z^*\right.\\ &\quad \left. + \langle\eta^{0*}c^{0*}u^{0*}|_{z^*=0}\rangle\right] - \frac{K_h}{\omega L^2}\partial_{x^*}\int_{-h^*}^{0} c^{00*}_{x^*}\mathrm{d}z^* + \mathcal{O}(\epsilon^3).\end{aligned} \quad \text{(C.3)}$$

Repeating the same procedure for the third and fourth terms of Eq. (C.2) gives,

$$\begin{aligned}&\left\langle \partial_{y^*}\int_{-h^*}^{\epsilon\eta^*}\left(\epsilon c^*v^* - \frac{K_h}{\omega L^2}c^*_{y^*}\right)\mathrm{d}z^*\right\rangle\\ &= \epsilon^2\partial_{y^*}\left[\int_{-h^*}^{0} c^{00*}v^{10*} + \langle c^{04*}v^{14*} + c^{12*}v^{02*}\rangle\ \mathrm{d}z^* + \langle\eta^{0*}c^{0*}v^{0*}|_{z^*=0}\rangle\right]\\ &\quad - \frac{K_h}{\omega L^2}\partial_{y^*}\int_{-h^*}^{0} c^{00*}_{y^*}\mathrm{d}z^* + \mathcal{O}(\epsilon^3).\end{aligned} \quad \text{(C.4)}$$

Using Eqs. (C.3) and (C.4) in Eq. (C.2), collecting leading-order terms and transforming back in to dimensional form gives,

$$\begin{aligned}&\partial_x\left(\int_{-h}^{0}\left[u^{10}c^{00} + \langle u^{14}c^{04} + u^{02}c^{12}\rangle\right]\mathrm{d}z + \langle\eta^{02}u^{02}c^{0}|_{z=0}\rangle\right.\\ &\quad \left. - K_h\int_{-h}^{0} c^{00}_{x}\mathrm{d}z\right)\\ &+\partial_y\left(\int_{-h}^{0}\left[v^{10}c^{00} + \langle v^{14}c^{04} + v^{02}c^{12}\rangle\right]\mathrm{d}z + \langle\eta^{02}v^{02}c^{0}|_{z=0}\rangle\right.\end{aligned}$$

$$-K_h \int_{-h}^{0} c_y^{00} \mathrm{d}z \Big) = 0. \tag{C.5}$$

Next, using the relations,

$$(c^0, c^{00}, c^{04}) = a(\tilde{c}^{0a}, \tilde{c}^{00a}, \tilde{c}^{04a}), \text{ and } c^{12} = a\tilde{c}^{12a} + a_x\tilde{c}^{12a_x} + a_y\tilde{c}^{12a_y},$$

and defining the following components:

$$(T^{xa}_{M_0}, T^{ya}_{M_0}) = \int_{-h}^{0} \boldsymbol{u}_h^{10}\tilde{c}^{00a}\ \mathrm{d}z, \quad (T^{xa}_{M_2}, T^{ya}_{M_2}) = \int_{-h}^{0} \left\langle \boldsymbol{u}_h^{02}\tilde{c}^{12a}\right\rangle \mathrm{d}z,$$

$$(T^{xa_x}_{M_2}, T^{ya_x}_{M_2}) = \int_{-h}^{0} \left\langle \boldsymbol{u}_h^{02}\tilde{c}^{12a_x}\right\rangle \mathrm{d}z, \quad , (T^{xa_y}_{M_2}, T^{ya_y}_{M_2}) = \int_{-h}^{0} \left\langle \boldsymbol{u}_h^{02}\tilde{c}^{12a_y}\right\rangle \mathrm{d}z$$

$$(T^{xa}_{M_4}, T^{ya}_{M_4}) = \int_{-h}^{0} \left\langle \boldsymbol{u}_h^{14}\tilde{c}^{04a}\right\rangle \mathrm{d}z, \quad (T^{xa}_{\text{surface}}, T^{ya}_{\text{surface}}) = \left\langle \eta^{02}\boldsymbol{u}_h^{02}\tilde{c}^{0a}|_{z=0}\right\rangle,$$

$$(T^{xa}_{\text{diff}}, T^{ya}_{\text{diff}}) = -K_h \int_{-h}^{0} (\tilde{c}_x^{00a}, \tilde{c}_y^{00a})\ \mathrm{d}z, \quad D_{K_h} = -K_h \int_{-h}^{0} \tilde{c}^{00a}\ \mathrm{d}z,$$

we can write the total horizontal sediment transport vector $\mathbf{T} = (T^{xa}, T^{ya})$ as

$$(T^{xa}, T^{ya}) = (T^{xa}_{M_0}, T^{ya}_{M_0}) + (T^{xa}_{M_2}, T^{ya}_{M_2}) + (T^{xa}_{M_4}, T^{ya}_{M_4}) + (T^{xa}_{\text{surface}}, T^{ya}_{\text{surface}}) + (T^{xa}_{\text{diff}}, T^{ya}_{\text{diff}}). \tag{C.6}$$

Collecting terms that result from horizontal diffusivity explicitly, together with advective contributions that exhibit diffusive behaviour, we can define a diffusivity matrix $\mathbf{D}^a$ for the sediment availability $a(x, y)$ as

$$\mathbf{D}^a = \begin{pmatrix} D_{K_h} + T^{xa_x}_{M_2} & T^{xa_y}_{M_2} \\ T^{ya_x}_{M_2} & D_{K_h} + T^{ya_y}_{M_2} \end{pmatrix}.$$

Using these results, the condition of morphodynamic equilibrium becomes an elliptic equation for the sediment availability $a(x, y)$ as

$$\nabla \cdot (\mathbf{D}^a \nabla a + a\mathbf{T}) = 0.$$

References

Chernetsky, A.S., Schuttelaars, H.M., Talke, S.A., 2010. The effect of tidal asymmetry and temporal settling lag on sediment trapping in tidal estuaries. Ocean Dyn. 60 (5), 1219–1241.

Cushman-Roisin, B., Beckers, J.-M., 2011. Introduction to Geophysical Fluid Dynamics. Academic Press.

Ensing, E., de Swart, H.E., Schuttelaars, H.M., 2015. Sensitivity of tidal motion in well-mixed estuaries to cross-sectional shape, deepening, and sea level rise. Ocean Dyn. 933–950.

Friedrichs, C.T., Armbrust, B.D., de Swart, H.E., 1998. Hydrodynamics and equilibrium sediment dynamics of shallow, funnel shaped tidal estuaries. In: Dronkers, J., Scheffers, M.B.A.M. (Eds.), Physics of Estuaries and Coastal Seas, (PECS 1996), pp. 315–327.

Friedrichs, C.T., Hamrick, J.M., 1996. Effects of channel geometry on cross sectional variations in along channel velocity in partially stratified estuaries. Buoyancy Eff. Coastal Estuarine Dyn. 53, 283–300.

Geyer, W., Signell, R., Kineke, G., 1998. Lateral trapping of sediment in a partially mixed. In: Dronkers, J., Scheffers, M. (Eds.), Physics of Estuaries and Coastal Seas. PECS. Balkema, pp. 115–124.

Gockenbach, M.S., 2006. Understanding and Implementing the Finite Element Method. Society of Industrial and Applied Mathematics (SIAM), Philadelphia.

Huijts, K.M.H., Schuttelaars, H.M., de Swart, H.E., Valle-Levinson, A., 2006. Lateral entrapment of sediment in tidal estuaries: an idealized model study. J. Geophys. Res. 111 (C12), C12016.

Jay, D.A., Talke, S.A., Hudson, A., Twardowski, M., 2015. Estuarine turbidity maxima revisited: Instrumental approaches, remote sensing, modeling studies and new directions, vol. 68. Elsevier B.V.

de Jonge, V.N., Schuttelaars, H.M., van Beusekom, J.E.E., Talke, S.A., de Swart, H.E., 2014. The influence of channel deepening on estuarine turbidity levels and dynamics, as exemplified by the Ems estuary. Estuarine, Coastal Shelf Sci. 139, 46–59.

Kim, Y.H., Voulgaris, G., 2008. Lateral circulation and suspended sediment transport in a curved estuarine channel: Winyah Bay, SC, USA. J. Geophys. Res. 113 (9), 1–15.

Kumar, M., Schuttelaars, H.M., Roos, P.C., Möller, M., 2016. Three-dimensional semi-idealized model for tidal motion in tidal estuaries: an application to the Ems estuary. Ocean Dyn. 66 (1), 99–118.

van Maren, D., van Kessel, T., Cronin, K., Sittoni, L., 2015. The impact of channel deepening and dredging on estuarine sediment concentration. Cont. Shelf Res. 95, 1–14.

Murray, A.B., 2003. Contrasting the goals, strategies, and predictions associated with simplified numerical models and detailed simulations. In: Prediction in Geomorphology, pp. 1–15.

Nayfeh, A.H., 2007. Perturbation Methods. Wiley-VCH Verlag GmbH.

Schramkowski, G.P., Schuttelaars, H.M., De Swart, H.E., 2002. The effect of geometry and bottom friction on local bed forms in a tidal embayment. Cont. Shelf Res. 22, 1821–1833.

Schuttelaars, H.M., de Jonge, V.N., Chernetsky, A.S., 2013. Improving the predictive power when modelling physical effects of human interventions in estuarine systems. Ocean Coastal Manage. 79, 70–82.

Soulsby, R., 1983. Physical Oceanography of Coastal and Shelf Seas. Elsevier Oceanography Series, vol. 35. Elsevier.

Souza, A.J., 2013. On the use of the Stokes number to explain frictional tidal dynamics and water column structure in shelf seas. Ocean Sci. 9 (2), 391–398.

Talke, S., de Swart, H., Schuttelaars, H., 2009a. Feedback between residual circulations and sediment distribution in highly turbid estuaries: an analytical model. Cont. Shelf Res. 29 (1), 119–135.

Talke, S.A., De Swart, H.E., De Jonge, V.N., 2009b. An idealized model and systematic process study of oxygen depletion in highly turbid estuaries. Estuaries Coasts 32 (4), 602–620.

Van Rijn, L.C., 1993. Principles of Sediment Transport in Rivers, Estuaries and Coastal Seas. Aqua Publications, p. 690.

Vreugdenhil, C.B., 1994. Numerical Methods for Shallow-Water Flow. Springer Netherlands.

Weilbeer, H., 2008. Numerical simulation and analyses of sediment transport processes in the Ems-Dollard estuary with a three-dimensional model. Sediment Ecohydraulics 30, 447–462.

Winant, C.D., 2007. Three-dimensional tidal flow in an elongated, rotating basin. J. Phys. Oceanogr. 37 (9), 2345–2362.

Winant, C.D., 2008. Three-dimensional residual tidal circulation in an elongated, rotating basin. J. Phys. Oceanogr. 38 (6), 1278–1295.

Zimmerman, J.T.F., 1992. On the Lorentz linearization of a nonlinearly damped tidal Helmholtz oscillator. Proc. Koninklijke Nederlandse Akademi 95 (1), 127–145.